eman ta zabal zazu
Universidad del País Vasco
Euskal Herriko Unibertsitatea

BILBOKO
INGENIARITZA ESKOLA

ESCUELA
DE INGENIERÍA DE BILBAO

MÁSTER UNIVERSITARIO EN INTEGRACIÓN DE LAS ENERGIAS RENOVABLES EN EL SISTEMA ELECTRICO

TRABAJO FIN DE MÁSTER

IMPACT OF WIND GENERATION ON LINE PROTECTION

Estudiante *Castañón, Méndez, Alberto Joaquín*
Director *Eguia, López, Pablo*
Departamento Departamento de Ingeniería Eléctrica
Curso académico *2019-2020*

Bilbao, 08, Septiembre, 2020

Abstract:

Renewable energy-based generation like wind and solar farms present a different response to short circuit than conventional synchronous generators due to their coupling trough power electronics-based inverters. Those so called Inverted Based Resources (IBR) behave like current sources as opposed to voltage sources and their short circuit current is highly determined by their control system. This fault current is generally limited to around 1.2 p.u. and is characterized by the lack of an expected negative sequence current (I2) due to most current control philosophies only taking in account positive sequence even in the presence of unbalanced faults. Protection Units that are based on I2 for fault recognition like Directional Sequence Overcurrent or Faulted Phase Selectors (FID) are foreseen to particularly suffer the lack of I2 expected from traditional Synchronous Generation. Modern Grid Codes specify advanced Low Voltage Ride Through (LVRT) requirements, including I2 control. Besides sequence components, Faulted Phase Selector algorithms makes use of incremental quantities concept to successfully identify faulted phase. Incremental quantities theory is based on the superposition principle, which is also expected to suffer in presence of IBRs. Present work goal is to provide a good understanding of the IBR phenomena that impacts protection engineering and to put to test different protection functions under IBR presence.

Keywords: Wind energy, inverter control, protection relays, negative sequence, incremental quantities, faulted phase selector

Resumen:

La generación basada en energía renovable, como parques eólicos o solares presentan una respuesta ante cortocircuito diferente a los generadores síncronos convencionales debido a su acoplamiento a la red mediante inversores basados en electrónica de potencia. Estas llamadas fuentes de generación basados en inversores (IBR) se comportan como fuentes de intensidad, no como fuentes de tensión y su intensidad de cortocircuito está determinada en gran medida por su sistema de control. Esta intensidad está generalmente limitada alrededor de 1.2 p.u. y está caracterizada por una falta de componente de secuencia inversa (I2) debido a que la mayoría de filosofías de control actuales toman en cuenta solo la secuencia positiva aún en presencia de faltas desbalanceadas. Debido a esto se prevé que funciones de protección que están basadas en I2 para reconocer faltas como Sobre-Intensidad Direccional de Secuencia o Selectores de Fase en Falta (FID) sufran la falta de este componente que se esperaría de generadores convencionales. Los códigos de red modernos requieren una capacidad para soportar huecos de tensión que incluyen control de I2. Además de utilizar componentes de secuencia, los selectores de fase en falta hacen uso del concepto de cantidades incrementales para operar. La teoría de cantidades incrementales está basada en el principio de superposición, que también se espera que sea impactado en presencia de IBRs. El objetivo del presente trabajo es proveer una descripción del impacto de las IBRs en la ingeniería de protecciones y poner a prueba diferentes funciones de protección en presencia de IBRs.

Palabras Clave: Generación eólica, control de inversores, relevadores de protección, secuencia inversa, cantidades incremental, selector de fase.

Contents

List of Tables

List of Figures

List of Acronyms

Acronym	Meaning
AG	Asynchronous Machine
CSC	Couple Sequence Control
DFIG	Double Feed Induction Generator
DFT	Discrete Fourier Transform
DSC	Decoupled Sequence Control
DSRF	Double Synchronous Reference Frame
EESG	Electronically Excited Synchronous Generator
FID	Faulted Phase Selector
GSC	Grid Side Converter
I1	Negative Sequence Current
I2	Positive Sequence Current
IBR	Inverter Based Resource
LVRT	Low Voltage Ride Trough
PLL	Phase Lock Loop

PMSG	Permanent Magnet Synchronous Generator
PWM	Pulse Width Modulation
RDFT	Recursive Discrete Fourier Transform
RSC	Rotor Side Converter
SSC	Stator Side Converter
V1	Positive Sequence Voltage
V2	Negative Sequence Voltage
VSC	Voltage Source Converter

1. Introduction

Governments around the globe are striving to comply with their goals of renewable energy share in their energy mix. Protection engineers and relay manufacturers are in need to review the impact that a grid with increased introduction of Inverter Based Resources (IBRs) will have on the performance of their protection algorithms. [1] Reviews the potential impact on Line Differential Protection (ANSI code 87L), on Distance Protection (21) and on Directional Ground Overcurrent Protection (67N), being the lack of a currently observed I2 the main driver for malfunction of protection units. This Final Master Work aims to describe basic inverter control theory and verify the impact of inverter control philosophy on Incremental Quantities based Faulted Phase Identification using MATLAB Simulink®.

2. Context

IBRs current contribution is heavily dependent on control strategy used [2]. Previous work has been done on modelling Wind Turbines (WT), but mostly focusing on active and reactive power grid code compliance for symmetrical voltage dips like in [3], [4], [5] or asymmetrical dips but complying to older grid codes like [6] in which no treatment is given to negative sequence components and often no mention of the control system used is done like in [7]. Given the benefits for both WT and the power grid of negative/positive sequence current injection during LVRT, grid codes have recently added this requirement, but most EMT models available in commercial software have fallen behind to include according strategies in their simulation blocks, as even stated on CIGRE 2018 release: “Most of the commercial software provides only positive-sequence current injection function” or “In the future a TSO may require that IBRs provides a negative sequence current in case of unsymmetrical faults mainly to ensure sufficient voltage recovery for all three phases” [8]. As reviewed in [9], [10], [11] and [12] a model whose control includes sequence decomposition is indispensable for asymmetrical short circuit response studies.

3. Objectives and Benefits

The benefit of the present work is that it presents a clear description of the control systems of IBRs for the two main kind of wind turbines, focusing on the characteristics that impact the behavior of those during fault, and therefore protection functions. Besides, the focus of the analysis is on the fault response during asymmetrical faults, while most of the currently available work focuses on symmetrical faults. In order to conduct a correct analysis of asymmetrical faults, standard models available on simulation software were modified to include LVRT characteristics required by latest grid codes. In the development of this work, three different simulation software packages were tested to achieve a reliable simulation of the two types of wind turbines, however none of them

offered a model with control modes updated to latest grid code requirements or commonly used protection methods. MATLAB Simulink® was finally selected due to the friendly environment offered to add features to the control scheme, which as stated is crucial to achieve simulations results that can actually compare to reality.

4. Inverted Based Resources

Independently of the primary source of energy, the impact of renewable energy on the electrical system is determined by the type of interface the generator has with the grid. Wind turbines (WTs) are usually classified in four types, according to the technology they use to interface to the grid and export generated power:

- **Type I** are squirrel-cage asynchronous generators (AG) directly connected to grid with a step-up transformer.

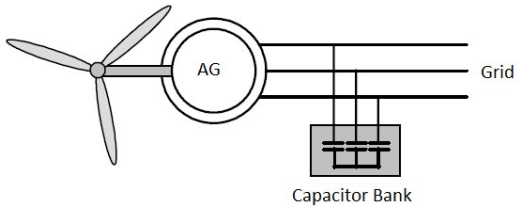

Fig. 1 Type I Wind Turbine [13]

- **Type II** are wound rotor asynchronous generators, which control rotor speed with a variable resistor.

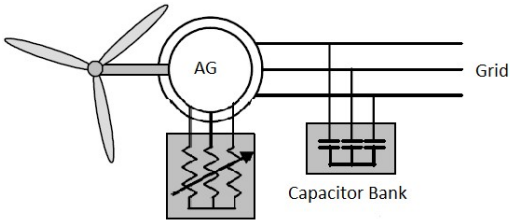

Fig. 2 Type II Wind Turbine [13]

- **Type III** turbines are double feed induction generators (DFIG), whose stator is directly connected to the grid and rotor is connected with a back to back power electronic based converter, with rating of around 25%-30% of the turbine rated power. Gearbox is still needed on this configuration.

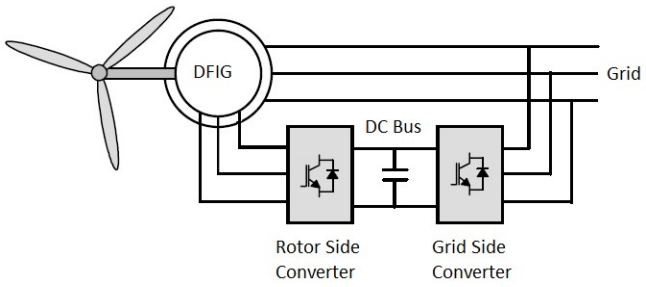

Fig. 3 Type III Wind Turbine [13]

- **Type IV** The full-scale WT mainly consists of a variable speed-controlled generator, connected to the grid through a full-scale back-to-back power converter, as it is shown in Fig. 4. The generator can be an asynchronous generator (AG), an electrically excited synchronous generator (EESG) or a Permanent Magnet Synchronous Generator (PMSG). The gearbox is not necessary in this case since the usually used generators can operate at lower speeds due to their high number of poles.

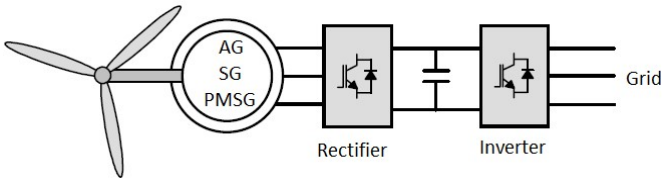

Fig. 4 Type IV Wind Turbine [13]

Type I is considered "fixed speed" since its synchronous speed is given by the machine number of poles and the grid frequency, which makes them inflexible and caused them to be replaced by the Type II [13]. The problem with type two is that adding resistors on the rotor side brings efficiency down as the extra energy form wind speed changes id dissipated on those resistors. Due to this reason, these two designs have been abandoned by the industry and Type III and VI currently dominate the market. Type III and IV can be classified as IBRs and in which this work will be focused on. A further division of the Type IV classification is made on [14] since recent developments already available on the market include full converter machines equipped with gearbox but this work will take all full converter equipped machines as one single Type IV category.

4.1. IBR Control

Before jumping into the electrical portion of the Type III and Type IV WTs an introduction of the basic aspects of commonly used control strategies for mechanical portion will be done:

• Turbine yawing.

This control consists on the rotation of the turbine along its vertical axis, in order to align its "face" or turbine's plane of rotation to the wind flow for maximum energy extraction. Modern turbines employ electric or hydraulic azimuth drives consisting of a motor and gearbox, a ring gear and a yaw controller [9].

• Pitch control.

The fraction of power converted from wind power P_{air} to mechanical power P_m is determined by the air density ρ, wind speed v and power coefficient C_p (1).

$$P_m = C_p * P_{air} = \frac{1}{2} C_p \rho v^3 \quad (1)$$

Where C_p is a function of pitch angle β, and tip-speed ratio λ.

Pitch control acts on β to regulate power extraction, it is important to mention that the relationship between β and C_p is non-linear and control most take it into account.

Early introduced WTs like Type I, made use of the above-mentioned control strategies to control turbine speed at a given operation point, but allowable deviation couldn´t go further than 1 %. However, maintaining constant speed under diverse wind conditions causes huge stresses on mechanical components. Variable-speed turbines (with rotor speed variation of up to 30% of rated rotor speed) have since been introduced and have captured the majority of the market. These variable-speed turbines employ a number of different methods to achieve their goals, while both mechanical (changing of gear ratios) and electrical methods (frequency converters) are feasible for speed changing, in practice electrical methods are preferred since they offer faster and more reliable methods of speed control. Variable-speed turbines have reduced dynamic loading on the mechanical as well as electrical systems, and also increase the time spent operating at optimal performance levels [15].

4.2. Power Converter

As previously stated, currently most used WTs are Type III and IV which make partial or full use of electronic based power converters. Power converters can be classified per their topology in Current Source Converters or Voltage Source Converters (VSC); per their commutation method, phase-controlled, (typically using thyristors and natural commutation synchronized with the grid voltage) or Pulse Width Modulation (PWM) using forced commutated devices; and per their number of conversion cells, like single cell converters (like neutral point clamped multilevel converters) or a multicell converter (like cascaded H-bridge or interleaved converters) [9]. Among this classification, the standard solution is the PWM-commutated multilevel VSC, which allows better control of the injected power and harmonics and employ standard power devices.

4.3. Voltage Source Converter Control

In order to review the control strategies of the before mentioned power VSC, one basic concept for Space Vector Control is needed. For an easier analysis and control of a three sinusoidal phases system, two mathematical transformations are used to treat it as a two-phase time-invariant orthogonal one, by changing the reference frames in which the system is represented. This reference frame change is achieved with the use of the Clarke and Park transformations.

Clarke Transformation: Also called α,β transformation. It allows to change between two different reference frames, the abc coordinate reference frame to the αβ0 reference frame. Both reference frames are shown in Fig. 5, where the αβ plane holds all the symmetrical vectors, this means, vectors with no zero sequence, or those vectors in which $v_a + v_b + v_c = 0$. On three-wire systems with no ground connection, as it is usually used for WTs, no component is expected on the 0-axis of the αβ0 frame, which is aligned with the space diagonal of the abc reference frame.

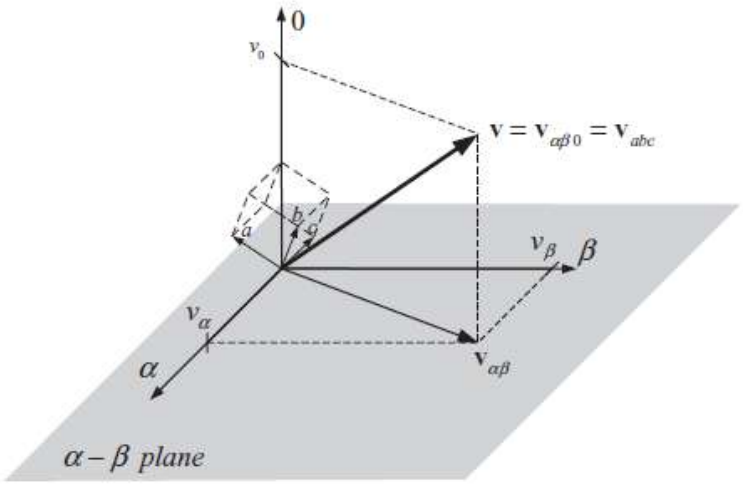

Fig. 5 Graphical representation of the αβ0 reference frame [15]

If the α-axis is aligned to the a-axis, and disregarding the zero component we have the conversion matrix shown in (2), in which the amplitude of the transformed components, either voltage or current is maintained.

$$\begin{bmatrix} i_\alpha \\ i_\beta \end{bmatrix} = \frac{2}{3} \begin{bmatrix} 1 & -\frac{1}{2} & -\frac{1}{2} \\ 0 & \frac{\sqrt{3}}{2} & -\frac{\sqrt{3}}{2} \end{bmatrix} \begin{bmatrix} i_a \\ i_b \\ i_c \end{bmatrix} \quad (2)$$

Park Transformation: Also called d,q transformation. It allows to change between two orthogonal axis reference frames which are displaced from each other by an θ angle. In this case, it is used to change from the αβ0 reference frame to a synchronous or dq0 reference frame, which is based on

two orthogonal dq axis rotating at frequency ω, which are placed at the $\theta = \omega t$ angular position on the αβ plane. Fig. 6 adds the mentioned dq0 reference frame to the previously seen graphical representation of the abc and αβ0 reference frames.

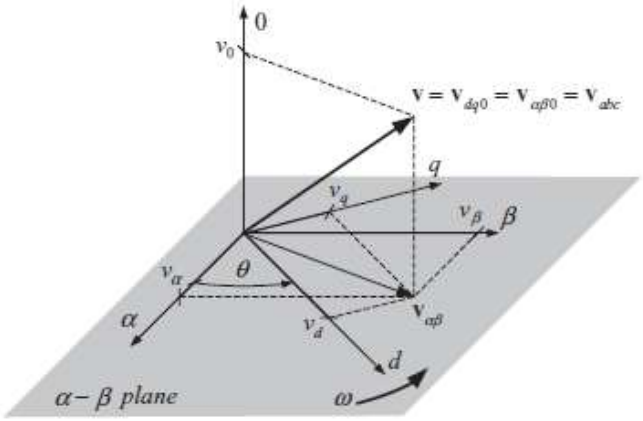

Fig. 6 Graphical representation of the dq0 reference frame ***[15]***.

If the d-axis is at an angle θ (rotation angle) to the α axis, and disregarding the cero axis, we have the following conversion matrix.

$$\begin{bmatrix} i_d \\ i_q \end{bmatrix} = \begin{bmatrix} \cos(\theta) & sin(\theta) \\ -sin(\theta) & \cos(\theta) \end{bmatrix} \begin{bmatrix} i_\alpha \\ i_\beta \end{bmatrix} \quad (3)$$

As a result of the above-mentioned reference frame shift. The signals represented on an static (αβ0) reference frame, which were time variant (sinusoidal), now appear as time invariant since the new reference frame (dq0) is also rotating at synchronous speed.

A graphical two-dimensional representation of applying both Clarke and Park transformations is shown on Fig. 7 for a more practical understanding of this concepts.

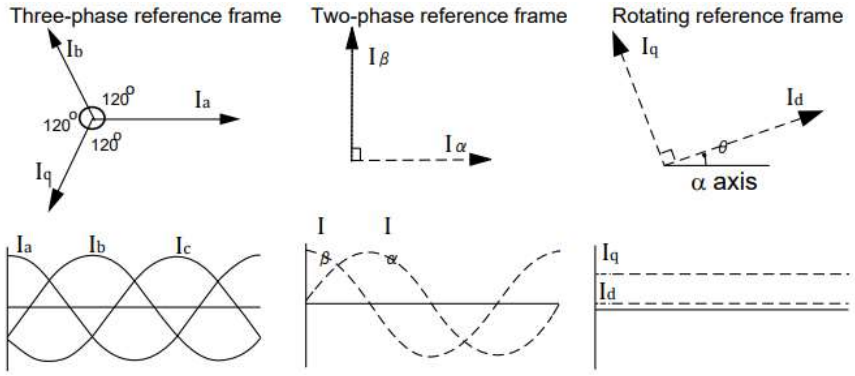

Fig. 7 Reference Frames Transformation ***[16]***

By applying this transformation, three phase AC currents and voltages can be controlled as two DC currents independently by classical Proportional Integral (PI) controllers as will be shown for each WT Type in the following section. Since the d axis is aligned with the measured ac grid voltage phasor and this results in a zero value of the q axis component of the measured voltage as illustrated in Fig. 7. this strategy enables independent control of active and reactive power, and dc and ac voltages [17]. However, classical PI controllers have two main disadvantages. The PI controller is unable to track a sinusoidal reference current without an appreciable steady-state error and has a poor disturbance rejection capability. The reason for this is the inadequate performance of the integrator when the disturbance varies periodically[17]. Proportional-resonant controllers need only Clark Transformation to operate at static two-phase reference frame and bring different advantages and disadvantages but are not the mainly adopted solution by the industry so were left out of the scope of this analysis. A good insight on resonant controllers can be found on [18]. Present work is focus on PI controller's strategy.

Fig. 8 shows the connection of a Voltage Source Converter to the grid through a coupling reactance (R and L).

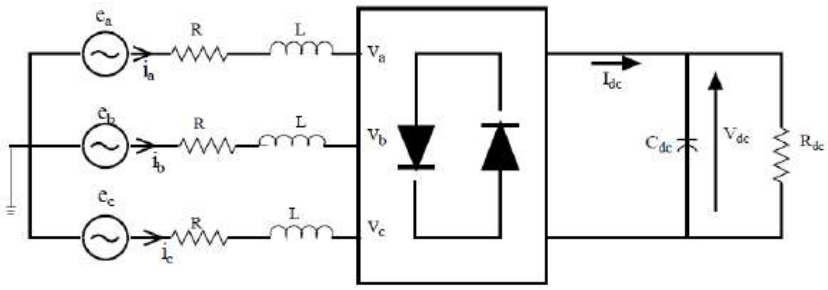

Fig. 8 VSC Coupling Inductor Scheme

Relations among phase voltage and phase currents in the coupling reactance represented in the abc reference frame, are given by the following equations:

$$e_a - V_a = R \cdot i_a + L \frac{di_a}{dt} \quad (4)$$

$$e_b - V_b = R \cdot i_b + L \frac{di_b}{dt} \quad (5)$$

$$e_c - V_c = R \cdot i_c + L \frac{di_c}{dt} \quad (6)$$

Which can be transformed in the dq reference frame and written as follows:

$$e_d - V_d = Ri_d + L \frac{di_d}{dt} - \omega_s L i_q \quad (7)$$

$$e_q - V_q = Ri_q + L\frac{di_q}{dt} + \omega_s L i_d \quad (8)$$

Where ω_s is the grid angular frequency. These two equations are the principle of the VSC control to be used for Type III and IV WTs. They also show that the d and q axes voltages are interdependent due to the frequency voltage cross coupling terms $\omega_s L i_q$ and $\omega_s L i_d$. Being equations (7) and (8) the basis for the current control or inner loop shown in Fig. 9. 888

Based on instantaneous power theory, active (P) and reactive power (Q) can also be given in dq axes as follows:

$$P = (e_d i_d + e_q i_q) \quad (9)$$

$$Q = (-e_d i_q + e_q i_d) \quad (10)$$

By aligning e_d or grid voltage to the phase a axis, or making angle θ shown in Fig. 6 equal to zero, no $e_q$component is present, and the reference for active and reactive power can be derived from equations (9) and (10) [17].

$$i_{d\_ref} = \frac{P_{ref}}{e_d} \quad (11)$$

$$i_{q\_ref} = \frac{Q_{ref}}{e_q} \quad (12)$$

Which are used for the outer control loop shown in Fig. 9.

Based on previously described model, the control philosophy for a voltage source inverter is shown in Fig. 9. Where through monitoring voltage across the coupling inductance, the control system can generate current references to manipulate power levels. This control strategy is applicable for both Type III and IV WTs and needs to be kept in mind in the following paragraphs.

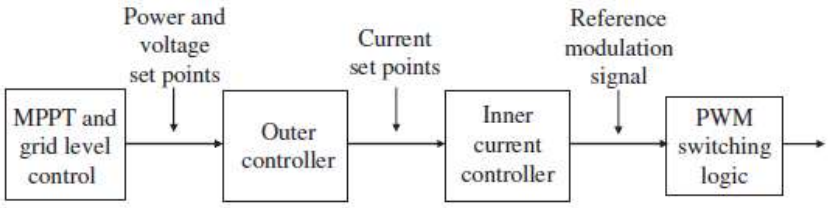

Fig. 9 Overall cascaded control structure of a voltage-source inverter [17]

MPPT stands for Maximum power point tracking for wind turbine generators and can be extended to solar PV generators.

In order to get the θ angle needed for the reference frame transformation different grid synchronizing techniques can be used, which can be classified into two main groups, namely the frequency-domain and the time-domain detection methods. Among the frequency-domain ones are the, the Discrete Fourier Transform (DFT) and the Recursive Discrete Fourier Transform (RDFT). Among the time-domain detection methods, the most common one is by the use of a Phase Lock

Loop (PLL). A PLL is a closed-loop system in which an internal oscillator is controlled to keep the time of some external periodical signal by using the feedback loop. A deeper insight on a PLL structure can be found in [15]. On this work, PLL will be used in the models which will be described lately.

As seen in Fig. 9, the output of the control loop is the modulation voltages, which the PWM translates in a switching sequence for the converter power electronics, a deeper review of the PWM technology can be seen in [19]. The aim of a PWM in power generation is to shape the output of an inverter by controlling the width and frequency of the switching devices. The scope of this work will reach the input signals for the PWM leaving the conversion to AC inside the converter as a black box.

4.4. Full Scale Converter Wind Turbine (Type IV) Control

As it was previously mentioned, the full-scale converter of a Type 4 WT consists of a Grid Side Converter (GSC) and a Stator Side Converter (SSC) as shown in Fig. 10. Control strategy shown is based on the model of a PMSG based WT, in which when the q-axis is aligned to the rotor magnet flux (Ψ), the dynamic model in dq-reference frame can be described per the following equations:

$$u_{sd} = -R_s i_{sd} - L_s \frac{di_{sd}}{dt} - L_s \omega_r i_{sq} \tag{13}$$

$$u_{sq} = -R_s i_{sq} - L_s \frac{di_{sq}}{dt} + L_s \omega_r i_{sd} + \omega_r \Psi \tag{14}$$

Where u_{sd}, u_{sq}, i_{sd}, i_{sq} are stator voltage and currents in dq reference frames, R_s is the stator resistance and L_s is the stator inductance, and Ψ is the magnet flux.

The electromagnetic torque is given by (11).

$$T_e = \frac{3}{2} p \Psi i_{sq} \tag{15}$$

where p is the pole pairs, from which can be concluded from that the torque of the generator, as well as the output active power, can be controlled by controlling the q-axis stator current.

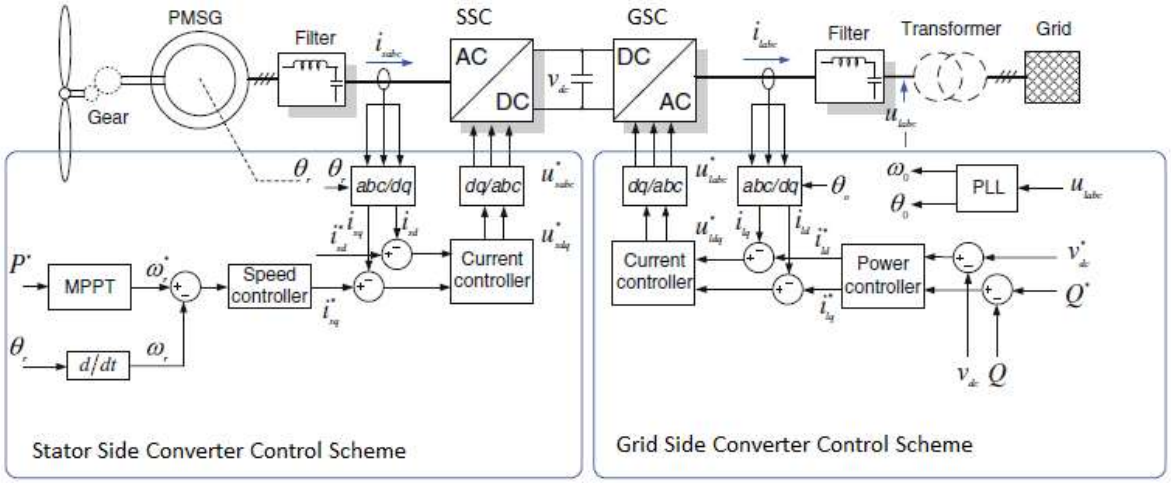

Fig. 10 Type IV WT Control Scheme [20]

Control Scheme shown in Fig. 10 follows the logic seen in Fig. 9 for both SSC and GSC. Where * indicates a reference signal.

The purpose of the SSC is to control Torque to match P requirements and to keep Q at a minimum. ω_r^* is derived from the P^*input sent by the Park Controller to the WT. ω_r^* is translated to i_{sq}^* by the speed controller (outer loop), which is compared with the measured i_{sq} and gives a reference voltage u_{sdq} for the PWM to control de SSC output (inner loop).

The purpose of the GSC is to control the voltage at the V_{dc} bus and the Q interchange with the grid (outer loop). Since the d_{axis} is aligned with the Grid voltage vector, V_{dc} is controlled trough i_{sd} and Q trough i_{sq} (inner loop).

4.4.1. Outer and Inner Loop

Fig. 11 shows a deeper insight of the actual loops inside of the Power or Speed Controller Blocks (Outer Loops) and the Current Controller Blocks (Inner Loops) shown in Fig. 10. As previously stated, the outer loop takes reference of P or V_{dc}, Q or V_{rms} and creates the reference on i_{dq} terms for the inner loop to operate. DC Bus Capacitor shown in Fig. 10 acts as an energy storage, rising V_{dc} when more P is being generated by the PMSG than injected to the grid by the VSC and vice versa, therefore V_{dc} can be taken as a measure of P as seen in the GSC control i_d loop in Fig. 10. Q and V_{rms} references are created in the outer loop depending on the park controller operation mode, Voltage Control or Power Factor control.

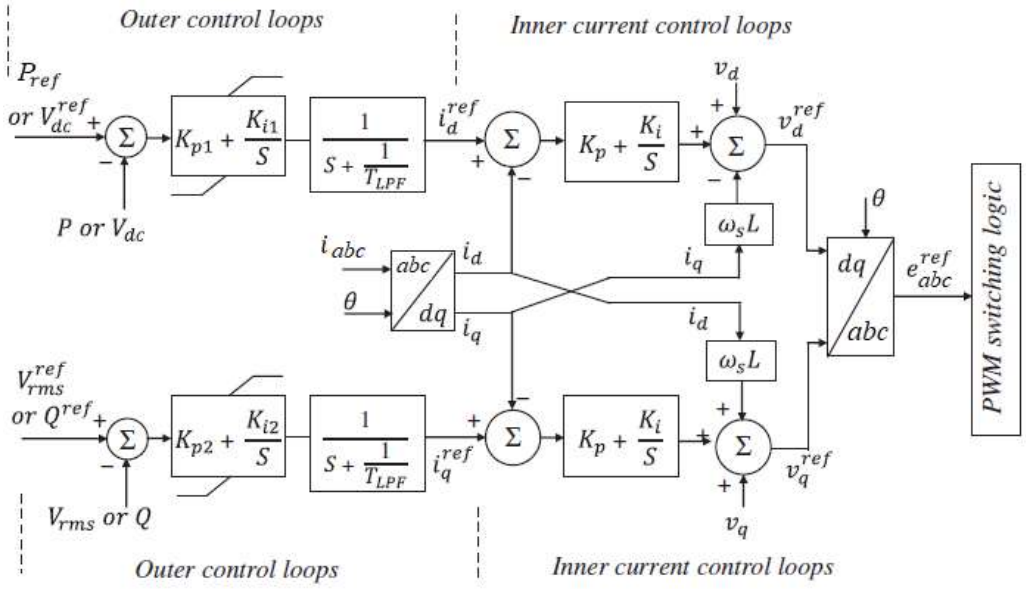

Fig. 11 VSC Outer and Inner Current Control Loops [17].

After the outer control loop has created the reference i_d^{ref} and i_q^{ref}, inner control loops operates according to equations (7) and (8) to generate v_d^{ref} and v_q^{ref} by comparing to measured v_d and v_q and adding coupling component $-\omega_s L i_q$ and v$\omega_s L i_d$, as seen in Fig. 11 PI controller gains are calculated based on the coupling reactance R and L values.

4.4.2. Type IV WT control in Double Synchronous Reference Frame

Control configuration shown in previous section is design to operate on a balanced grid condition. However, in presence of asymmetrical faults, negative-, positive- and zero- (if grounded) sequence voltage components appear at the terminals of the inverter. Under this conditions, accurate current regulation requires control, of both positive sequence current (I1) and negative sequence current (I2), therefore is typically a Double Synchronous Reference Frame (DSRF) required, where currents are first transformed to the αβ reference frame and then sequence components are extracted by either notch filters or delayed phase shift transformation, with the disadvantage of increasing computational complexity [21]. Once the components are extracted, in grid codes where negative-sequence reactive current injection requirement is not explicitly made, inverter manufacturers usually suppress the negative-sequence component and inject a positive-sequence current component only. Control philosophies were I2 is suppress are called Coupled Sequence Control (CSC) and when I2 is taken in account are called Decoupled Sequence Control (DSC) in [22], terminology that will be used along this work. Under CSC inner control loop, double frequency power oscillations arise, which degrades the system performance and reduces the system reliability [23]. An explanation of the origin of this double frequency oscillations can be found in [24], [25]

and [23]. In order to eliminate these oscillations, a DSC is needed, which treats sequence components on separate loops and injects a negative sequence current whose amplitude is proportional to the negative sequence terminal voltage [26]. When grid codes require negative sequence current injection, a dual-sequence control scheme with a negative-sequence dq2 rotating reference frame is required as shown in Fig. 12, where the inner control loop PI controllers are duplicated to act on the negative and positive sequence components of the dq currents and voltage and the AC reference voltage for the converters is comprised of both components. This negative sequence component control is required since when a grid fault appears, the objectives of VSC interface are, besides delivering average active and reactive power to the grid as specified in the Grid Code, also to minimize instant active and reactive power ripple, to deliver balanced grid currents, to control maximum grid current value, and to minimize dc-link voltage ripple [12] . These objectives are pursuit by control strategy by injecting currents that attempt to minimize negative sequence voltage while maximizing positive sequence voltage, tending to restore the voltage profile as if no sag has occurred, to the extent of the inverter physical limitations [11]. From the power grid point of view a pure positive sequence current injection in the presence of unbalanced voltage leads to higher phase over voltages, which should be avoided [10]. A good comparison of WT fault current behavior under CSC or DSC is done in [27] and [10]. It is important to mention that for the correct operation of a grid-connected inverter under unbalanced conditions a more complicated phase extraction method than the classical PLL is required for extracting positive and negative sequence. Such more complicated PLL schemes like the Decoupled Double Synchronous Reference Frame (DDSRF), Dual Second Order Generalized Integrator (DSOGI), Cascaded Delayed Signal Cancellation Phase Locked Loop PLL, etc. add complexity to the design and implementation of the control scheme [28], [29]. A good explanation of the DSOGI is given in [15] and [29].

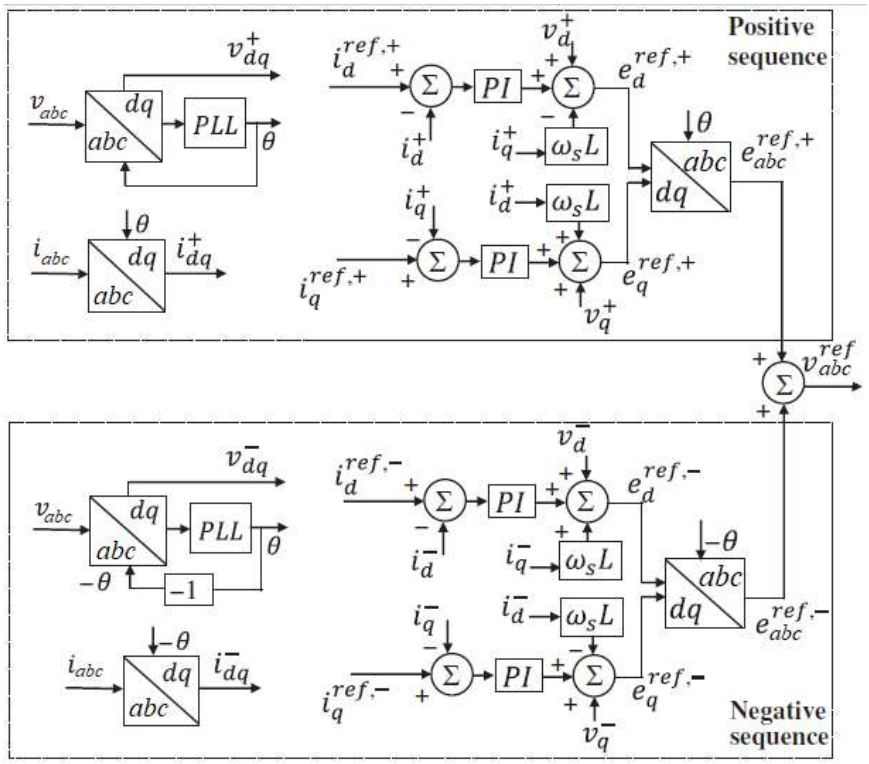

Fig. 12 Voltage-source inverter positive- and negative-sequence inner current control *[17]*

4.5. DFIG Wind Turbine (Type III)

As previously stated, DFIG machines evolved from the idea of controlling an Asynchronous Machine speed, which was not possible with the first Type I WTs, since the rotor on a squirrel cage machine is not accessible. This was firstly achieved by interfering rotor winding with resistors and later by the DFIG machine. In order to explain the principle of how a DFIG machine achieves this flexibility in operation the basics for induction machine needs to be reviewed:

For an Induction Machine, the difference between being a motor or functioning as a generator lies in the speed of the rotor. In general, if the rotor speed is higher than the synchronous speed then it behaves as a generator (stator rotating magnetic field follows rotor magnetic field), and if the rotor speed is less than the synchronous speed (rotor magnetic field follows the stator one) it becomes a motor. The synchronous speed is determined by the line frequency and the number of poles of the stator winding (16).

$$N_s = \frac{60f}{p} \tag{16}$$

Previously mentioned behavior can be seen in Fig. 13, from which many interesting characteristics of the induction machine can be deduced but for our purpose we will focus on the fact that at synchronous speed no torque is delivered as a motor or used as a generator.

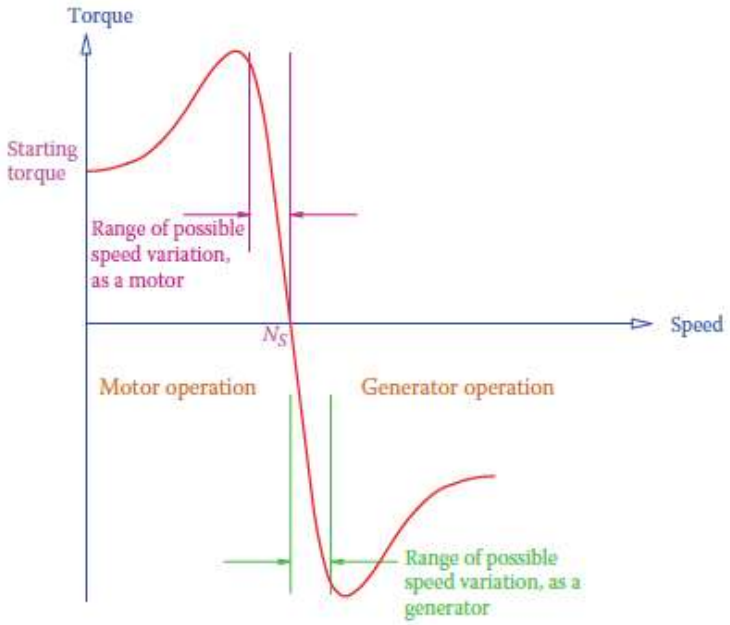

Fig. 13 Torque-speed characteristic of a Three Phase Induction Machine [19].

The difference between the speed of the rotating magnetic field (synchronous speed, N_s) and the rotor speed (N) is called the slip speed, and the ratio of this difference to the synchronous speed is called slip (S), as shown in following formula:

$$S = \frac{N_s - N}{N_s} = 1 - \frac{N}{N_s} \tag{17}$$

When an induction generator works, a low-frequency AC current, proportional to the machine slip flows through the rotor windings. With fundamental frequency varying from a few Hz to a few tens of Hz [30].

$$f_{slip} = f_s - f_r = f_s\left(1 - \frac{f_r}{f_s}\right) = sf_s \tag{18}$$

where f_s is the synchronous frequency (50 or 60 Hz) and f_r is the rotor rotational frequency proportional to the rotor speed. This concept of rotor current at slip frequency is the base for understanding the functioning of the DFIG machine.

DFIG based WTs (Type III) present two main advantage over Squirrel Cage (Type I) and Resistor Controlled (Type II) Induction Machines. First, it is capable of controlling P and Q output, while the previous ones need to consume Q. Second, a DFIG WT can work at a wider range of wind speeds. For example, typical wind speed range of Type I and II WTs goes from 4 m/s (9 mph) to 20 m/s. In comparison, a DFIG can work in the range of 3 to 24 m/s wind speeds. With the lower end extra 3 m/s range not being significant but the upper extra range being pretty important [19]. An additional advantage of the Type III over the Type II WT is the reduction in losses since instead of adding resistances to the rotor circuit, power can be injected back to the grid.

As seen in Fig. 14, on a DFIG, stator is connected directly to the step-up transformer that connects the wind turbine to the grid, while the stator is connected through a bidirectional back-to-back AC-DC-AC converter. This converter is composed of a Rotor Side Converter (RSC), a DC Bus and a Grid Side Converter (GSC).

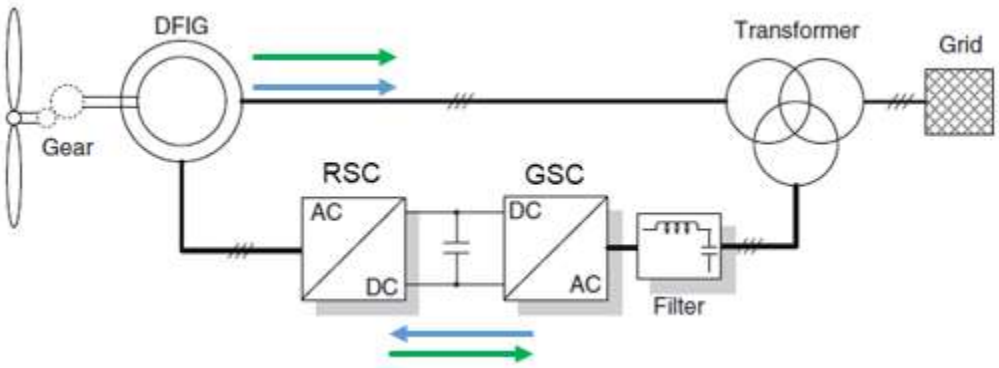

Fig. 14 Type III WT (DFIG Based) Basic Scheme [20].

As it was mentioned, the most important advantage is related to the DFIG ability to operate below its synchronous speed and at up to 30 to 40% higher than its synchronous speed. Speeds below the synchronous speed are called sub-synchronous, and those above the synchronous speed are called super-synchronous speed.

As long as the generator speed is higher than the synchronous speed, the DFIG could behave as a common induction machine, but in order to increase its range of operation to higher winds speed, at this called super-synchronous operation, the alternating current in the rotor winding is rectified to DC and inverted to feed the grid. This current removal reduces generated torque and allows to keep generating energy at a wider range of wind speeds. In this operation mode, power is transmitted to the grid trough both the stator and the rotor as shown in Fig. 14 in green power flow.

Beyond increasing the wind speed operation range at super-synchronous speed, as it was mentioned, the DFIG can even work at speed below the synchronous one, at which a common induction generator would behave as a motor. If the rotor of a common induction generator speed drops down to the synchronous speed, slips goes to zero, no current is induced and power generation goes to cero, if speed keeps going down, negative slip is produced and the generator becomes a motor drawing current from the grid. On a DFIG, if slip goes down to cero or below, the

back-to-back converter draws current from the grid and injects it into the rotor to keep the stator generating. This current is injected at an opposite polarity to the current that the stator field would induce in the rotor to work as a motor, canceling it out and forcing the opposite polarity to keep the stator rotating magnetic field following the rotor magnetic field and generating, this is equivalent to adding mechanical energy to the generator. In this operation mode, power transmitted to the grid is the one produced by the stator minus the one drawn by the rotor but still positive as shown in blue in Fig. 14

A comparison of the extended range of operation reached is shown in Fig. 15. Where dashed purple line shows usual behavior of an induction machine like the one shown in Fig. 13. Blue lines show lighter manipulation of current and red one drawing or injecting more current. Lines in the upper part of the picture show how for super-synchronous speed, torque can be maintained constant at different speeds by extracting more or less current from the rotor. Lines on the lower section show how the zero-torque point at which the machine would turn into a generator is shifted to the left as much current is injected into the rotor, allowing for a wider range of operation.

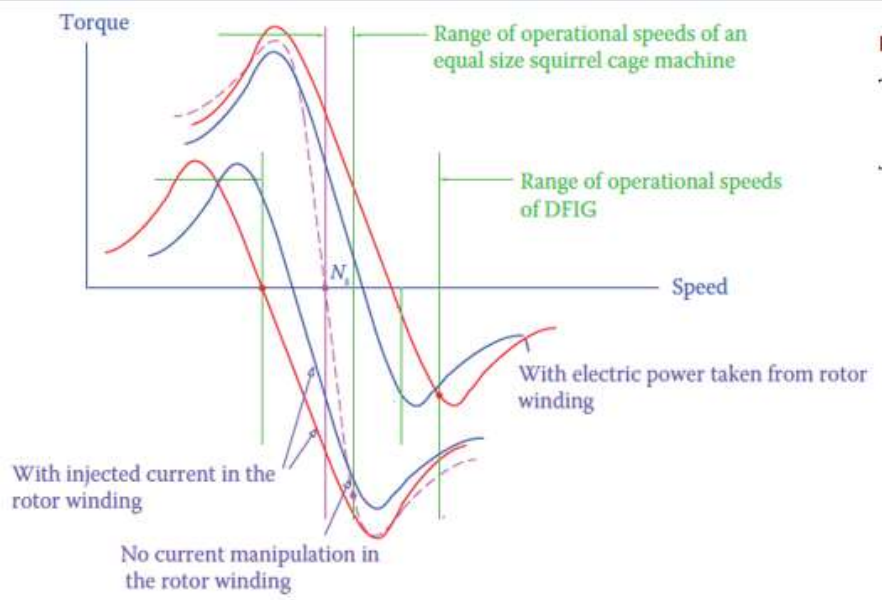

Fig. 15 Extension in the range of operational speeds in a DFIG [19].

Above comparison of the DFIG machine to an asynchronous machine is valuable to understand why can the Type III WT have an extended range of operation with a low loss, taking into account the frequency of the injected current into the rotor circuit to match slip speed. However, since the RSC allows for complete control of the current, phase shift can also be achieved. A detailed explanation of the comparison of a DFIG to a Synchronous machine is done in Chapter 7 of [31], where the following conclusions can be extracted to complete the analysis of a Type III WT capabilities. Controlling the magnitude of the rotor current component in phase with the stator voltage, controls the real power, while controlling the magnitude of the rotor current component out of phase with

the stator voltage, controls the reactive power. Being this capability to control reactive power the second advantage of the DFIG machine.

Vector control of a Type III WT is similar to the one of a Type IV on the already seen outer control loop, in which the active power reference (P_{dfig}) is given by the MPP and the DFIG positive sequence terminal voltage reference (V_{dfig}) by the park controller, it is in the inner loop where the difference between a Type IV and a Type III can be seen.

RSC controls P and Q flow from the stator of the DFIG to the grid. This is achieved by controlling the magnitude, frequency, and phase angle of the three-phase currents injected into the rotor by the duty ratio (PWM) control of the VSC. GSC regulates the DC link voltage by providing a path for the active power transfer (positive or negative) between the rotor side converter and the grid, besides providing additional reactive power support to the grid [30].

Now, applying reference frame conversion seen previously, DFIG control can be seen in Fig. 16, where i_{qr} and i_{dr} are the q- and d-axis currents of the RSC, i_{qg} and i_{dg} are the q- and d-axis currents of the GSC. RSC operates in the stator flux reference frame and the GSC operates in the stator voltage reference frame. Therefore in Fig. 16 scheme:

- i_{qr} is used to control $P_{dfig.}$
- i_{dr} is used to control V_{dfig}.
- i_{dg} is used to control V_{dc}.
- i_{qg} is used to control additional Q during faults.

These currents references, indicated by a (´) in Fig. 16 are used by the inner control loop to generate the modulated switching signals for the PWM controlled converters.

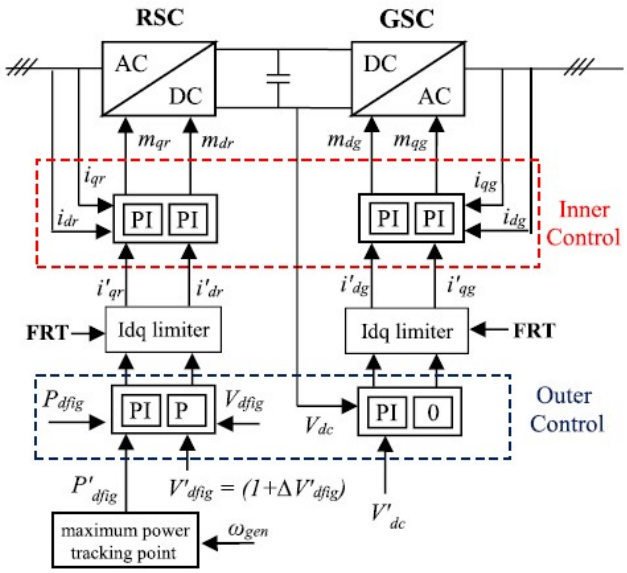

Fig. 16 DFIG Control Scheme [32]

5. Fault response of IBRs

5.1. DFIG Wind Turbine (Type III)

On a DFIG, stator terminals are directly connected to the grid. As a result, the initial transient response following a sudden voltage drop (as a result of grid fault) is dominated by the demagnetization of the induction machine which may result in high stator peak currents [27]. This stator overcurrent is transmitted, due to the magnetic coupling, and the laws of flux conservation, to the rotor windings [33]. These overcurrents, which can be up to three times the nominal value of the current, can damage the rotor and stator windings, but can be especially critical for the semiconductors of the RSC, that can reach a thermal breakdown [34]. A good vectorial explanation of this phenomena is given in [35]. Furthermore, the surge following the fault includes a "rush" of power from the rotor terminals towards the converter. As the grid voltage drops in the fault moment, SGC is not able to transfer the power from the RSC to the grid and therefore the additional energy goes into charging the DC bus capacitor, dangerously rising its voltage.

As analyzed in [13], on steady state, voltage on the stator creates a rotating magnetic flux proportional to the magnitude of this voltage, called direct flux. During faults, since voltage changes rapidly on the stator, a transient component of the flux arises to compensate for this change, which is fixed in respect to the stator and decays with time, varying with the current present in the rotor, this flux is called free flux.

Based on this interpretation, it can be stated that the voltage on the rotor is dependent on the own rotor currents and also the voltage induced by the stator fluxes $\vec{v}_o^r$, as described in following equation on stator reference:

$$\vec{v}_r^r = \vec{v}_o^r + R_r^{'} \cdot \vec{i}_r^r + L_r^{'} \frac{d}{dt} \vec{i}_r^r \tag{19}$$

Where $\vec{v}_r^r$ is the rotor voltage on rotor reference frame, $\vec{i}_r^r$ is the rotor current on rotor reference frame and $R_r^{'}$ and $L_r^{'}$ are the machine resistance and inductance. $\vec{v}_o^r$ is produced by three different components, namely direct, inverse and free voltage.

$$\vec{v}_o^r = \vec{v}_d^r + \vec{v}_i^r + \vec{v}_f^r \tag{20}$$

Direct component is caused by the direct component of the stator voltage through the direct flux and is proportional to the slip in magnitude and since this flux rotates with the stator, its frequency seen by the rotor is that of the slip (s), a few hertz.

$$\vec{v}_{rd}^r = \frac{L_m}{L_s} \cdot \vec{v}_d \cdot s \cdot e^{js\omega_s t} \tag{21}$$

Where L_m and L_s are mutual and stator inductances.

In case of an asymmetric fault, the inverse component of the stator voltage will also induce a rotating flux in opposite direction, which is called inverse flux, which rotates at almost twice the synchronous speed and therefore creates a higher voltage component:

$$\vec{v}_{ri}^{r} = \frac{L_m}{L_s} \cdot \vec{v}_i \ \cdot (2 - s) \cdot e^{-j(2-s)\omega_s t} \tag{22}$$

The component of the voltage induced by the free flux is proportional to the magnitude of the voltage sag on the stator and its frequency is that of the electrical speed of the rotor.

$$\vec{v}_{rf}^{r} = \frac{L_m}{L_s} j\omega \vec{\Psi}_{sf}^{r} \tag{23}$$

Where $\vec{\Psi}_{sf}^{r}$ is the free flux produced by the discontinuity on the stator flux caused by the fault, referenced to the rotor.

In order to protect RSC the most extended solution is based on the use of a protective circuit known as crowbar, as shown in Fig. 17. This device consists of a three-phase diode bridge for AC/DC conversion, and a switching device such as a GTO in series with a small resistance on the DC side. When an over-current condition is detected, the GTO is switched from the off to the on state and shorts the rotor windings, therefore bypassing and protecting the RSC [15], making most of the voltage drop to happen across the resistance and not on the RSC terminals, but also incapacitating Q and P control, leaving the DFIG working as a common induction machine, withdrawing reactive current from the grid, which is totally opposed to what fault support requires.

During asymmetrical faults [36], the higher risk faced by the DFIG is not the mentioned current peaks, but the torque pulsations that cause wear on the gearbox and the DC ripple that impact DC-link capacitor life cycle. This both effects are caused by the inverse flux.

Two main solutions are used to avoid crowbar activation and its subsequent loss of control. Demagnetizing control and DC Chopper. First solution consists on bypassing steady state control of the RSC during under voltage events to orientate RSC current injection towards reducing transient rotor currents and minimize occurrence of crowbar interruptions. Second solution consists on the addition of a DC Chopper connected on the DC Bus as shown in Fig. 17. This Chopper consists on a set of resistances installed in parallel to the DC converter capacitor, which in case of severe grid fault will limit over voltages in DC link, and these resistances will dissipate the energy that cannot be delivered to the grid due to the short circuit. Both overcurrent on the RSC and overvoltage on the DC bus which the Crowbar and DC Chopper try to avoid can be attributed to the excessive energy generated that cannot be transmitted into the grid during the faults, due to the voltage drop they generate.

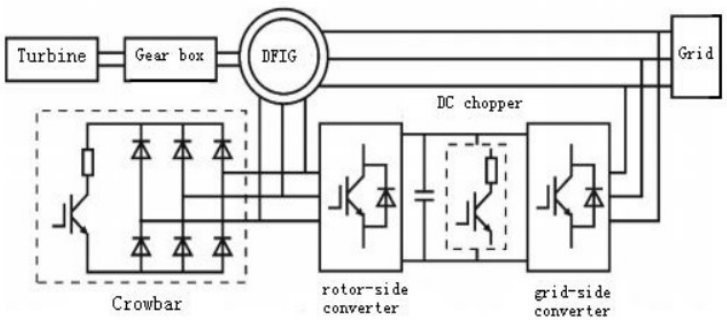

Fig. 17 Type III WT Protections Scheme [37]

A third solution for the usual loss of control during crowbar activation has been lately implemented. An active crowbar circuit, which is similar to the usual (passive) crowbar shown in Fig. 17, but interfered with IGBT switches instead of GTOs and therefore controllable. It bypasses the fault currents from RSC while still providing limited control during grid fault conditions. Providing reactive power support through the GSC to partially offset the Q consumed by the WT. This modern scheme is left outside of the scope of this study.

A study on the impact of crowbar activation is presented in Fig. 18 for a three-phase fault, where is worth noticing that with crowbar protection the fault current significantly drops down to a negligible value in two electrical frequency cycles, changing considerably the behavior.

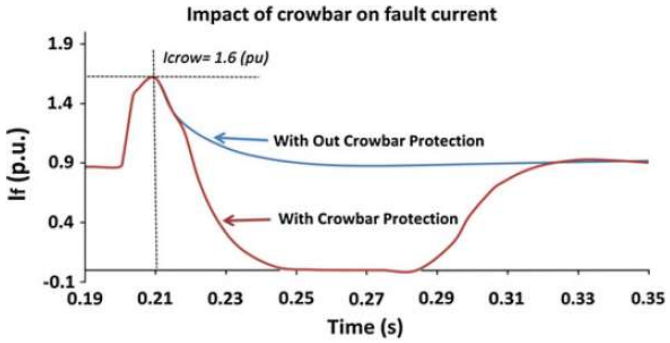

Fig. 18 Impact of crowbar on fault current [38].

Per the previously described behavior, in absence of the crowbar activation, it is expected than collective response as the initial current magnitude is large enough to get distance relays operated. Differential protection schemes should also be capable of detecting initial current. However, an overcurrent protection scheme may face issues due to protection coordination delays and the decaying response of such WTs.

5.2. Full Converter Wind Turbine (Type IV)

On a Full Converter interfaced WT, response to faults is totally dependent on the control structure. Generally, in case of Type-4 WTG, the initial short-circuit current is around 25 % of the rated current and this builds up in 2-4 cycle to reach a rated value of constant current [30]. If such WTs are not supported through some additional advanced control features then distance, differential, and overcurrent protection schemes are most likely to have functional problems. Therefore, control response to low voltage is strictly regulated by Grid Code as shown in Fig. 32. Since current is dependent on the control strategy, Type-IV WT might be represented as a current source almost right after fault inception. Due to these reasons, a higher focus on the control will be done for this WT type.

6. Line Protection Principles

Given the afore mentioned differences between a SG and IBR´s, being those mainly on I2 behavior, following protection principles were tested.

6.1. Negative Sequence Overcurrent (50Q)

This protection principle is based on the detection of I2 to detect asymmetrical faults and compares the module of I2 with a certain set point to declare a fault.

6.2. Negative Sequence Directional Overcurrent (67Q)

This principle makes use of the relative angular difference between I2 and V2 on the fault, since as seen in Fig. 19, I2 polarity changes depending on the fault location. In other words, it measures impedance seen on its line end and determines current direction from impedance having either a positive or negative value.

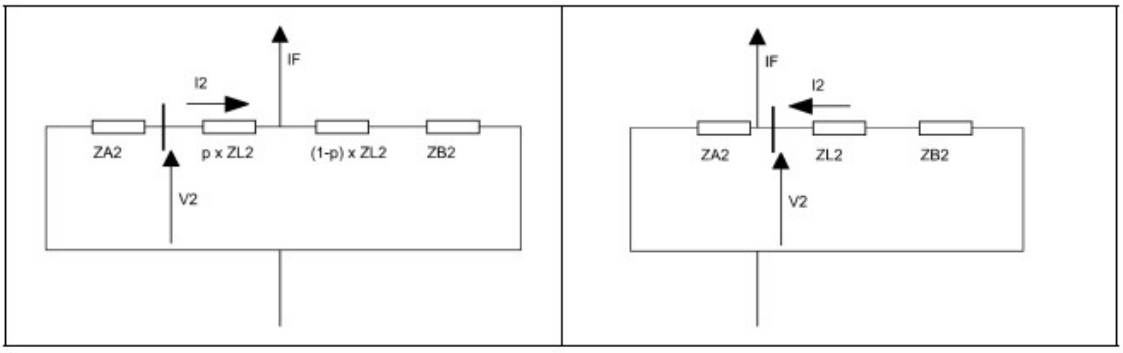

Fig. 19 Negative Sequence Network for a Forward or Backward Fault

6.3. Faulted Phase Identification Algorithm

6.3.1. Negative and positive Sequence Current Angle Comparison.

Distance Protection Relays incorporate a Faulted Phases Detector as part of the supervision units. This function follows two basic principles to identify fault type.

1. Low negative-sequence current component.
2. Low zero-sequence current component.

- If both conditions are fulfilled, fault is classified as a three-phase fault.
- If only condition 2. is fulfilled it means no connection to ground was established and fault is classified as a two-phase fault.
- If only condition 1. is fulfilled it means connection to ground was established and fault is classified as a single-phase or two-phase to ground fault.

In order to determine which phases are faulted, Φ angle is analyzed:

$$\Phi = arg(I_{a2}) - arg(\Delta I_{a1}) \quad (24)$$

Where:

I_{a2} is the negative-sequence current component referred to phase A.

ΔI_{a1} is the pure-fault positive-sequence current component referred to phase A.

Relation between positive and negative-sequence components provides fault classification according to following criteria Fig. 20.

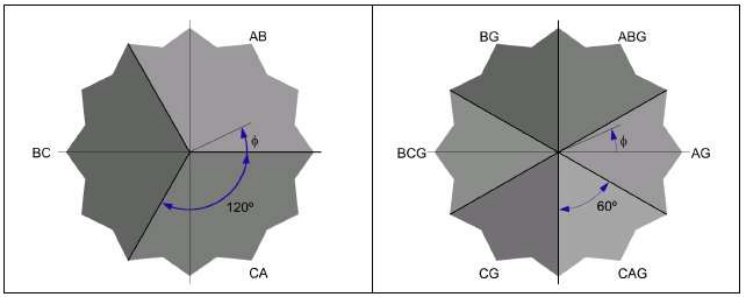

Fig. 20 Angular diagram for fault classification *[39]*.

6.3.2. Negative and Zero Sequence Current Angle Comparison.

The principle behind such criteria, as explained in [40], is that the angle by which I0 leads I2 during a fault (**φ**), is given by sequence network representing at a fault.

$$\boldsymbol{\varphi} = arg(I_{a2}) - arg(I_{a0}) \quad (25)$$

As an example, Fig. 21 and Fig. 22 show a AG and BCG fault respectably, where Z_f is the fault impedance.

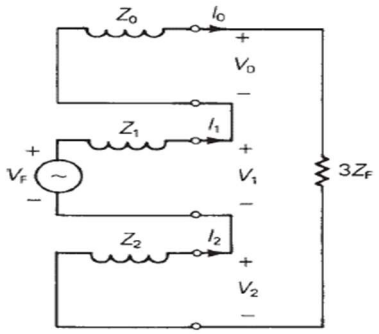

Fig. 21 Sequence Network for an AG Fault

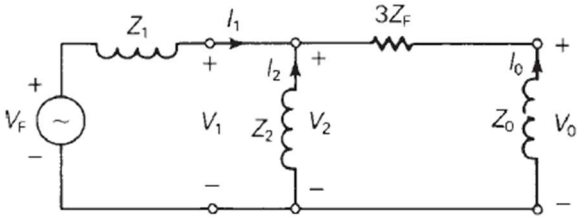

Fig. 22 Sequence Network for a BCG Fault

In Fig. 21, it can be seen that I0 and I2 at fault location have practically the same angle, taking in account that negative sequence (Z2) and zero sequence impedances (Z0) are fairly similar along the system. In Fig. 22 it is also shown how I0 and I2 are practically in phase, except for a case with high values of Z_f. Due to this reason the location of **ϕ** can be set to an area of -30° to 30° for AG or BCG faults and +30° to +90° for high impedance BCG faults. Extending this analysis to the rest of fault types and taking phase A angle as the reference for angle calculation following distribution of **ϕ** location can be deducted.

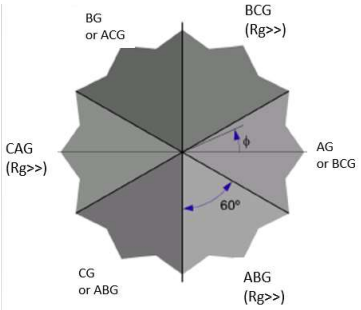

Fig. 23 φ location for ground faults.

6.3.3. Negative and Zero Sequence Voltage Angle Comparison.

Under weak infeed conditions, as usually happens with wind turbines, I2 level might not be enough to undergone a reliable phase angle comparison to other current sequence components. Under such circumstances voltage sequence components can be used. According to [41] and as shown in Fig. 21, for an AG fault, U1 and U2 have opposite phase angles, and according to Fig. 22, for a BCG fault they have same phase angle. As described in [42] , assuming same phase angle for all impedances across the system, which is fairly accurate, this characteristic can be used to differentiate a Phase to Ground (Ph-G) from a Phase to Phase to Ground (Ph-Ph-G) Fault. Furthermore, under Ph-G faults, U0 vector will be in line with the failed phase or with the healthy phase for Ph-Ph-G faults, therefore criteria shown in can be used to detect fault type.

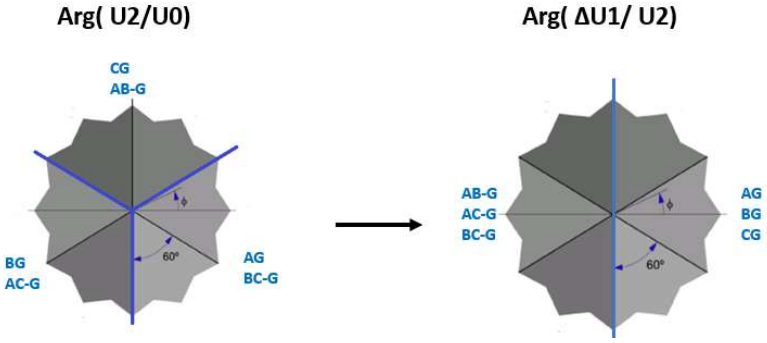

Fig. 24 Voltage sequence comparison

6.3.4. Negative and Positive Sequence Voltage Angle Comparison.

As shown in [43], in case weak source is connected through a Yg-Δ transformer, as is usually the case with wind turbines, ground current will be mainly cero sequence, making phase current look similar among them even for asymmetrical ground faults, which is known as the Bauch´s Paradox. In this case, current base methods for faulted phase selection might not be reliable and voltages can be used. As it was mentioned, and shown in Fig. 22, for a BCG fault, U1 and U2 have same phase angle. Given that the symmetrical components are referenced to a particular phase, if the angular difference between U1 and U2 is 0° (BCG), 120° (ACG) o -120°(ABG), this implies a Ph-Ph-G fault, if this is not the case, then a Ph-G fault is being seen and the corresponding phase is selected by the lower voltage.

6.4. Incremental, Superimposed or Delta Quantities

Faulted phase algorithm previously presented makes use of the so called Incremental, Superimposed or Delta Quantities theory to determine the ΔI_{a1} component, which allows to eliminate deviations due to pre-fault load conditions by splitting the fault network into a pre-fault and a pure-fault one. Subtracting a value of the signal, before a change (due to a disturbance or fault) from its corresponding value after the change will produce a signal that represents the change [44]. Following example illustrates the concept.

Considering the single-line diagram of Fig. 25, where a fault is applied through a resistance Rf at a distance m per-unit line length from the relay at the left bus.

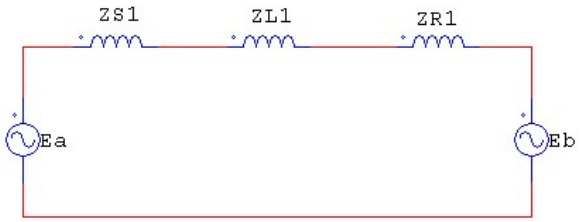

Fig. 25 Example System Single Line Diagram

Following the superposition principle, Faulted state Fig. 26 can be decomposed into a Pre-Faut Fig. 27 and a Pure-Fault Fig. 28 one.

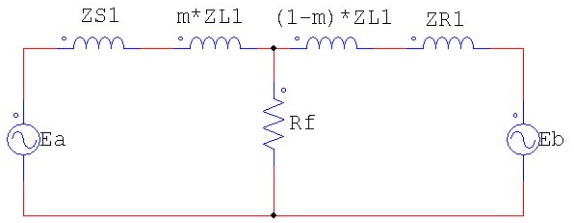

Fig. 26 Faulted Network

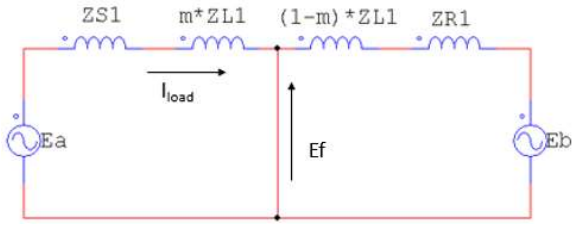

Fig. 27 Pre-Fault Network

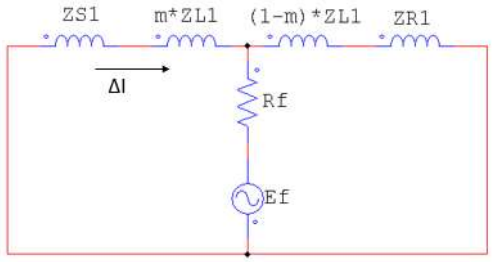

Fig. 28 Pure-Fault Network

Where the pure-fault network has the following characteristics:
a) Voltage sources must be short-circuited.

b) A voltage source, Ef, must be applied at the fault point, whose magnitude is equal to the voltage level existing at the fault location before application of the fault and its phase angle is opposite to that of the pre-fault voltage phase angle at the fault point.
The pure-fault network currents and voltages are zero before the fault. Therefore, any value they have due to a fault condition represents a change or delta quantity. For this reason, they are called incremental or superimposed quantities and are represented with a prefix Δ to indicate the change with respect to the pre-fault circuit values [45].

$$V = V_{pre-fault} + \Delta V \quad (26)$$

$$I = I_{pre-fault} + \Delta I \quad (27)$$

As previously stated, relays usually make use of both Sequence Components and Incremental Quantities Theories for its faulted phase selection algorithm. With the current increase of Renewable Energy contribution in generation it is important to make sure that the second principle is still valid on an IBR abundant grid.

7. Study Case

In order to test previously presented theory, the following power system has been taken from the detailed models in Matlab Simulink®, as shown in Fig. 29. The model consists of a voltage source behind an impedance representing the grid at 120 kV. A 30 km line has been split in two 15 km sections to represent a fault right in the middle of the line. A YgD1 power transformer is used to connect a 5 km cable at the MV side of the system, which is grounded through a zig zag transformer. A D11Yg power transformer is used to connect the low voltage side of the system in which an aggregated model of a Wind Park is masked inside the blue block on Fig. 29. This is the typical configuration of a Wind Park. Three fault locations were chosen for testing, at wind park terminals, at grid side of the line and middle of the line. System components ratings and details are given in Appendix A.

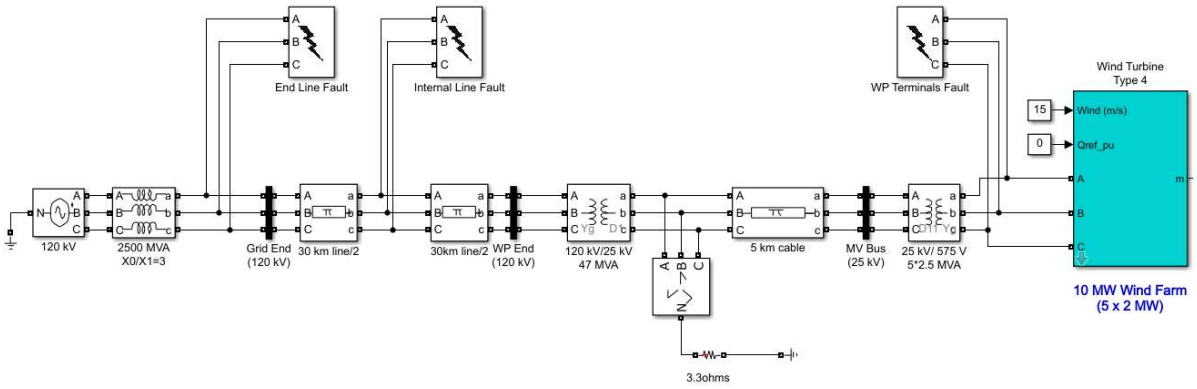

Fig. 29 Wind Turbine Test Power System

The difference between the Type III and Type IV models lies on the Wind Farm block shown in Fig. 29. Each of the models for the two WT types will be described more in detail in following sections.

7.1. MATLAB SIMULINK Type IV WT Detailed Model

The so-called *Synchronous Generator and Full Scale Converter (Type 4) Detailed Model* was used as a base to test Type IV WT response. Wind Farm block shown in Power System (Fig. 29) contains the model of the WT in Fig. 30. This model includes a) Induction Generator, b) SSC, c) GSC, d) Coupling Inductance and e) Filter. Rating have been adapted to match the aggregated model of a 5x 2 MW Wind Park. It is worth noticing that the SSC on this model is represented by a non-controllable simple diode rectifier since the interface to the grid is mainly the purpose of the GSC and therefore it is this converter the one of interest.

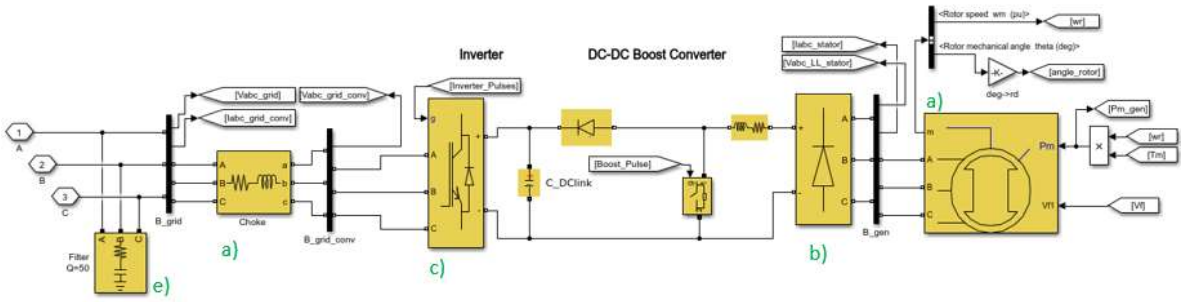

Fig. 30 Type IV Model Fully Interfaced Synchrnous Generator

In the case of the Type IV model the control block which is of interest for short circuit simulation is the GSC control shown in Fig. 31, which can be compared to previously presented Fig. 11 since a) Vdc regulator, represents the part of the outer loop in charge of creating the d current component reference in order to keep Vdc stable, b) is in charge of creating q current component reference to follow either a Q or V reference usually provided by park control, c) limits q output to avoid exceeding maximum rectifier current limit by given priority to d component (active power) and leaving the available rest to the q component (reactive power), d) represents the inner current control loop, whose purpose is to follow current references provided by the outer loop by applying (13) and (14) as previously reviewed, in order to compare to measured current and provide the voltage reference to the PWM generator that controls the GSC.

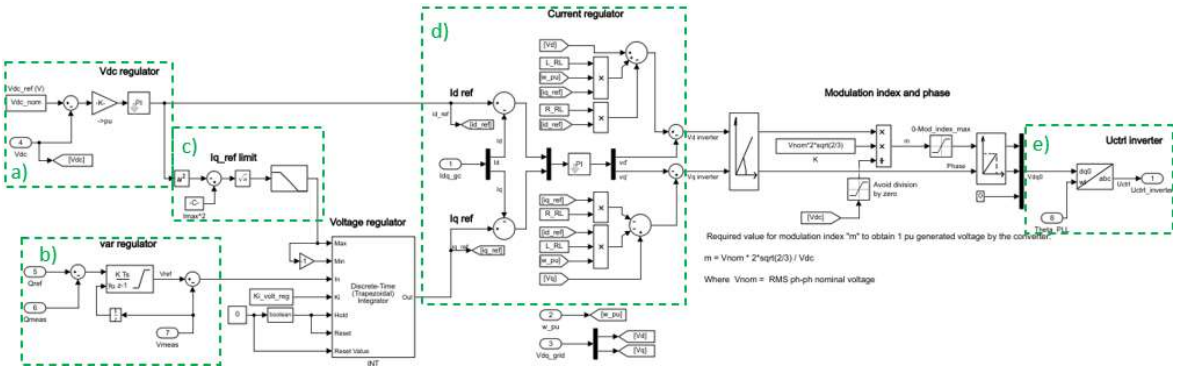

Fig. 31 Grid Side Converter Control of Type IV WT Model

7.2. Grid Code Requirements

Once the structure of the controllers has been introduced, the impact of the latest regulations on the design will be explained. Since present work is focused on protection principles, reactive current injection requirements on grid codes will be of main interest, leaving aside frequency or active power control.

As reviewed in [46], system operators in some countries (i.e., Germany, Denmark, England, Ireland, and Spain) impose reactive current injection requirements for the large IBRs interconnections to support the grid reliability under grid faults. This reactive current is the positive sequence current, which is essential to keep loads, especially induction machines and other generation units, running during the fault by adding to voltage level and rotor angle stability of conventional synchronous generators connected nearby the wind power plant [10]. The primary grid codes on LVRT mainly focused on the interconnection requirements under balanced grid faults. However, the most recent grid code, published in 2015 in Germany (VDE-AR-N 4120), as well as Spanish Grid Code have even considered the negative-sequence current injection during unbalanced faults. Negative sequence current injection as seen in previous sections bring the benefits of increasing individual phase voltages and reducing negative sequence voltage therefore, lowering grid voltage unbalance [47], not to mention the benefit provided for current protection algorithms by emulating more precisely the behavior of a Synchronous Generator under fault. Therefore, the need of present work to investigate the impact of both coupled and decoupled sequence control in protection algorithms. Latest draft of the Spanish Grid Code requires following structure for current injection under LVRT conditions.

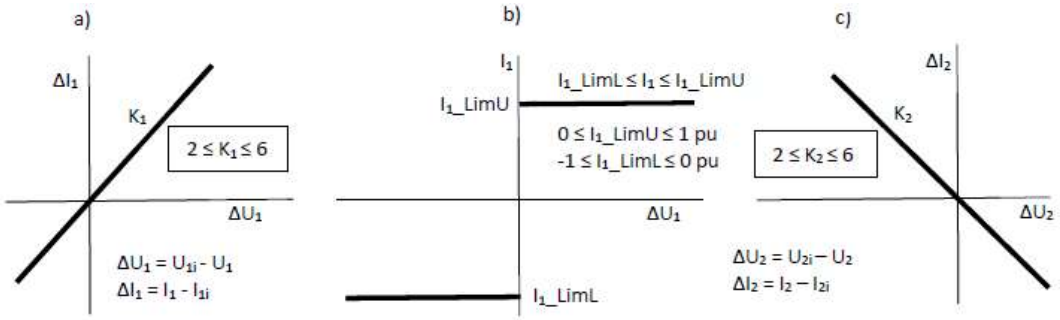

Fig. 32 Reactive and Negative Sequence Injection requirements per PO12.2 *[48]*

a) Additional required positive-sequence reactive current injection ΔI_1 as a function of positive-sequence voltage increase ΔU_1. b) Total reactive current I_1 injection limits. C) Additional required negative-sequence current injection ΔI_2 as a function of positive-sequence voltage increase ΔU_2.

All magnitudes are in per unit.

Where:

K_1: Positive-sequence current control gain.

ΔU_1: Positive-sequence voltage deviation.

U_{1i}: Positive-sequence voltage before perturbation.

U_1: Positive-sequence voltage.

ΔI_1: Positive-sequence current (reactive) deviation.

I_{1i}: Positive-sequence current (reactive) before perturbation.

I_1: Positive-sequence current (reactive).

K_2: Negative-sequence current control gain.

ΔU_2: Negative-sequence voltage deviation.

U_{2i}: Negative-sequence voltage before perturbation.

U_2: Negative-sequence voltage.

ΔI_2: Negative-sequence current deviation.

I_{2i}: Negative-sequence current before perturbation.

I_2: Negative-sequence current.

ΔI_1 and ΔI_2 injection is not required if generated power before perturbation is lower than 5% of the maximum capacity.

If RMS Voltage U at generator terminals is lower than 0,2 p.u. the blocking of power electronics is allowed, but must be reestablished after a maximum of 100ms after U comes back above 0,2 p.u.

Generation park must inject above required current according to following time limits see Fig. 33:

- Injection delay time (t_i) maximum 20ms.
- Response time (t_r) from injection start to 90% of required current corresponding to voltage deviation step of maximum 30ms.
- Establishment time (t_r) from injection start to reach a ±5% deviation band from set point of maximum 60ms.
- TSO Authority can agree to (tr) of up to 300ms on 30ms steps and (te) of up to 600ms in 60ms steps.

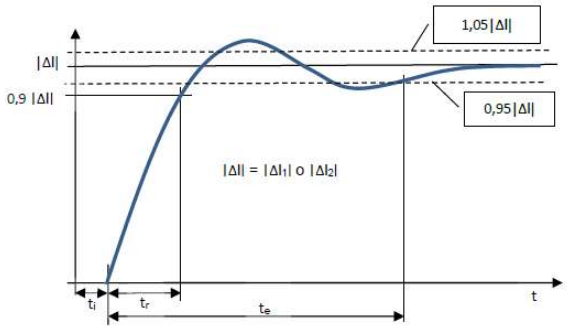

Fig. 33 Required time limits for LVRT Current Injection *[48]*

Regarding the post fault ramping up of the active power, Spanish Grid codes requires the following:

- If undervoltage level was **no lower than 0,2 pu**, active power must be ramped up to 95% of previous power **in less than 1 second**, and once U reaches 0,85 pu must reach 100% in maximum 2 additional seconds.
- If undervoltage level was **lower than 0,2 pu**, active power must be ramped up to 95% of previous power **in less than 3 seconds**, and once U reaches 0,85 pu must reach 100% in maximum 2 additional seconds.

7.3. Double Synchronous Reference Frame Control on Type IV Model

As stated before, in order to have a model that represents more accurately the behavior of WTs during fault, two main additions needed to be made to the standard model:

- Sequence Time Domain Decomposition (Fig. 34)
- LVRT (Fig. 37)

Sequence Decomposition is required for the PI based control to work under asymmetrical faults as previously explained. Control Scheme presented on latest section was modified to include negative sequence reactive current injection as per latest grid codes as shown in section 7.2. Two different methods of approaching negative sequence control are described in [12], namely the Vector Current Controller with Feedforward of negative sequence grid voltage in which the current controller is implemented in the positive reference frame, while the negative-sequence grid voltage is fed-forward and added to the reference voltage given by the controller. And the Dual Vector Current Control in which grid currents and voltage are separated in positive and negative sequence components, i_d and i_q references are calculated for both sequences and current controllers also duplicated for both sequences. This latest Dual Vector Current Control has been adopted.

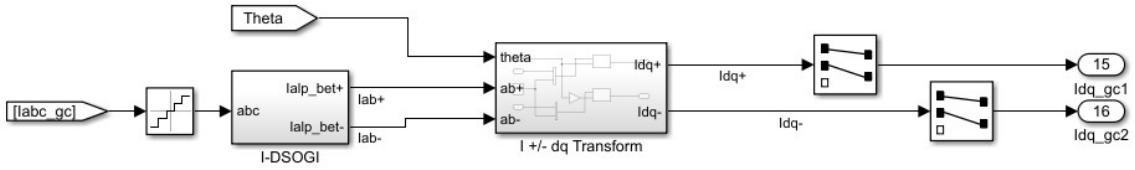

Fig. 34 DSOGI Based Time Domain Sequence Decomposition

As explained in [15], time domain d/q decomposition can be achieved with the use of a DSOGI. Fig. 34 shows the grid three-phase current set of signals entering the DSOGI Block to be split in positive and negative sequence alpha/beta reference system set, after this transformation, both positive and negative set can be transformed in their respective d/q system using the PLL calculated theta.

DSOGI block is shown in Fig. 35. This block is based on the Lyon method, which is a version of the Fortescue symmetrical components method adapted to the time domain which dictates that a alpha/beta system can be decomposed on its positive and negative sequence by the use of $[T_{\alpha\beta+}]$ and $[T_{\alpha\beta-}]$ transformation matrixes as shown in (28) and (29):

$$v_{\alpha\beta}^{+} = [T_{\alpha\beta+}]v_{\alpha\beta}; \quad [T_{\alpha\beta+}] = \frac{1}{2}\begin{bmatrix} 1 & -q \\ q & 1 \end{bmatrix} \tag{28}$$

$$v_{\alpha\beta}^{-} = [T_{\alpha\beta-}]v_{\alpha\beta}; \quad [T_{\alpha\beta-}] = \frac{1}{2}\begin{bmatrix} 1 & q \\ -q & 1 \end{bmatrix} \tag{29}$$

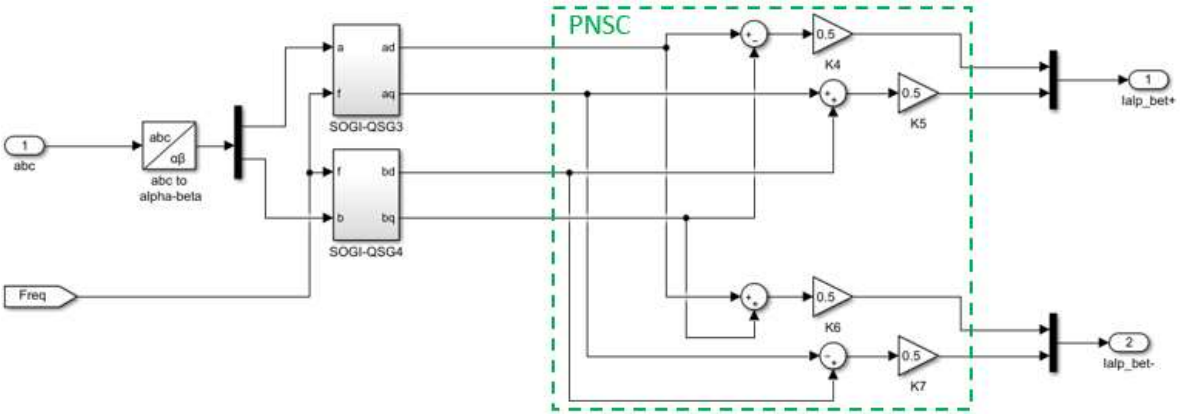

Fig. 35 DSOGI Block

The q component in (28) and (29) is actually a $q = e^{-j\pi/2}$ lagging phase-shifting operator applied on the time domain. This q is obtained by the use of a Second Order Generalized Integrator (SOGI) Quadrature Signal Generator for each of the alpha and beta signal, therefore the name of the DSOGI (Double SOGI).

On this scheme each SOGI outputs a set of two in-quadrature signals from their given alpha and beta sinusoidal, which are feed into the positive/negative sequence calculation net shown in Fig. 35, which applies (28) and (29). The benefits of using a DSOGI instead of a DDSRF is that no Decoupling Network is needed [15].

This decomposition scheme is duplicated for the current before entering the control loops, the result of this method is illustrated in Fig. 36, where the positive and negative alpha/beta components of the current and voltage during an asymmetrical fault are shown. On the first line on the figure, corresponding to the positive sequence current it can be seen how after fault inception at 0.03 sec only d component decreases while q component remains cero. On the second line both current negative components are non-existent before fault inception. On third and fourth line, corresponding to the voltage, it is shown how the d component of the positive sequence drops during fault and negative components arise due to the unbalanced.

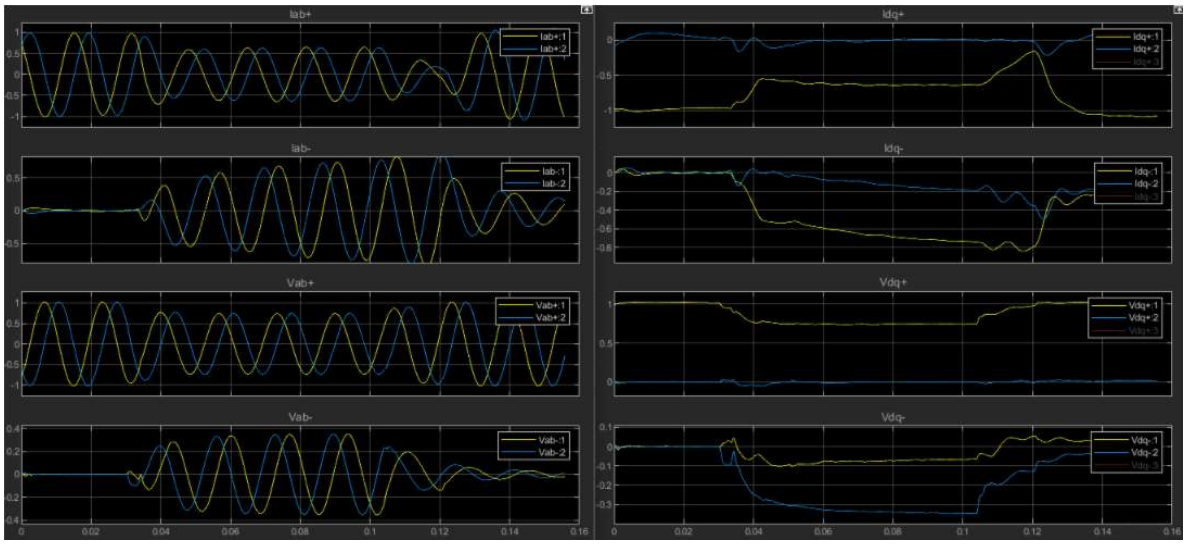

Fig. 36 Sequence Decomposition of Voltage and Current

Regarding the LVRT feature added to the control, it is designed to comply with the LVRT requirements shown in Fig. 32 and therefore takes in account both positive and negative sequence components. LVRT Mode current references are calculated as shown in Fig. 37

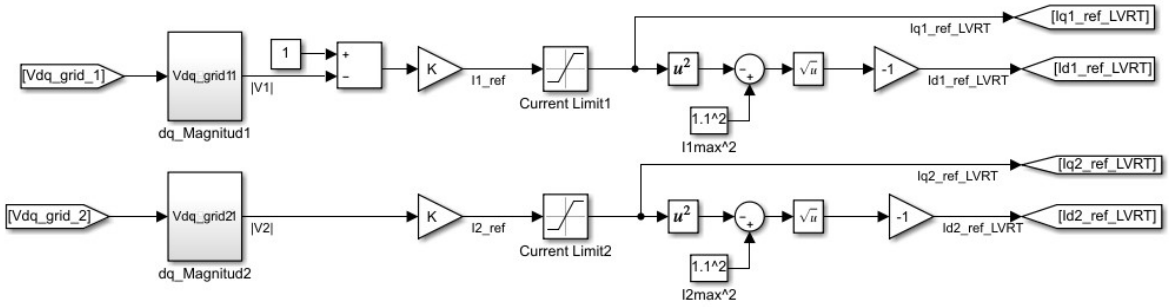

Fig. 37 LVRT Current References Calculation

Current references are taking from the steady state outer loop until a fault according to P.0. 12.2 criteria is declared, then current references are taken from the LVRT calculation.

Current references are calculated according to the Positive (V1) and Negative (V2) Sequence Voltage variation. Total current is limited to 1.1 (typical overcurrent limit for an inverter) and priority is assigned to reactive current injection (q component) on both sequences, assigning the available current before reaching the limit to active current (p component).

As stated in [49] it is not only the K current control gain factor asked for on Gird Codes that impacts a WT behavior under fault, it is also the inverter limits and how the d and q components are prioritized once this limit has been reached. Fig. 38 shows the Type IV fault response to an AG fault for a K=2 chosen. Regarding factor K impact, for a low K value, response might be totally reactive and no active power evacuation is done, which rises Vdc voltage to dangerous levels for the capacitor, a high K value on the other hand might not support voltage with reactive current as required.

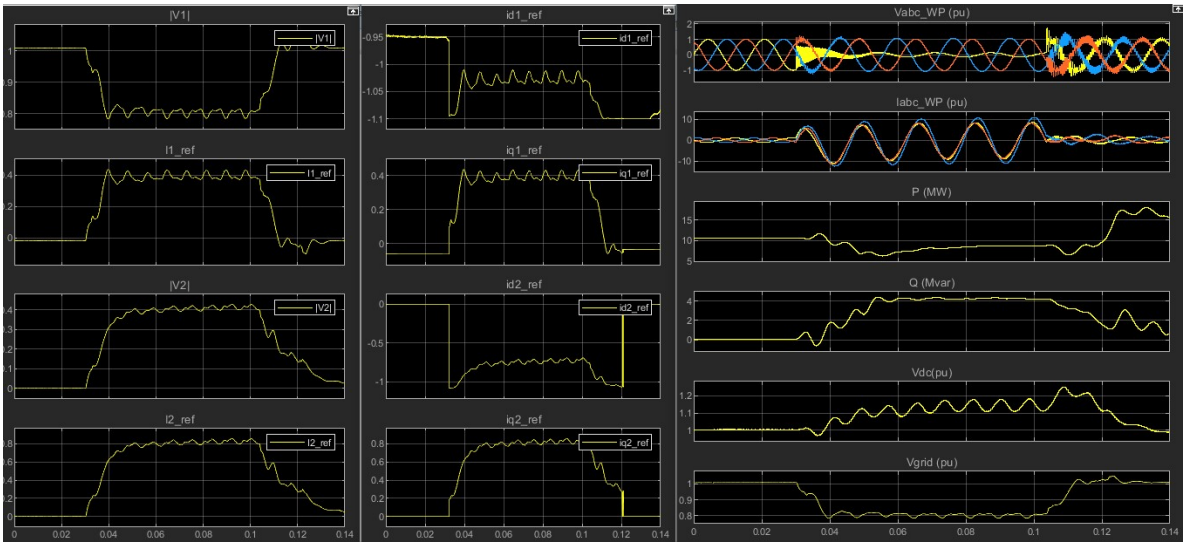

Fig. 38 Type IV response to AG. Reference a) calculations b) limiting and c) output

Left column shows |V1| and |V2| variations and their corresponding references I1_ref and I2_ref calculated accordingly. I1_ref (0.4) is double the |V1| variation (0.2), while I2_ref (0.8) is also double the |V2| variation (0.4). Center column shows reference split in d and q component, where iq1_ref is maintained at (0.4) and the rest is assigned to id1_ref component, (-1.025), likewise, iq2_ref is maintained at (0.8) and the left is assigned to id1_ref component, (-0.8). The impact of such calculation is seen on the power output where Q increases to 4 MVAr and P decreases to around 8 MW. Q injection change impacts voltage by supporting it from falling to 0.73 pu as it does if no voltage support LVRT strategy is used, but P reduction needed to accommodate extra reactive injection causes Vdc to raise up to 1.2 p.u.

A different LVRT control philosophy was developed aiming to mimic a SG response by injecting each Id+, Iq+, Id-, Iq- component according to their corresponding voltage component observed at generator terminals, inspired on the work done in [49] but no successful results were obtained for FID functions in different faults. As explained in [50], modern inverter´s LVRT control aim to comply with positive and negative reactive current required by grid codes, and are those requirements the ones who determine the angular position of I1 and I2, and not the voltage components angular positions as expected from a SG and reviewed on chapter 6. In other words, the impedance represented by the WT is modified by the grid codes requirements. In order for this impedance to emulate that of a SG, the WT control would need to detect the fault type and adjust I1 and I2 angular relation to I0 if traditional current based IFD schemes need to be used.

7.4. MATLAB SIMULINK Type III WT Model

The so-called *Wind Farm - DFIG Detailed Model* in MATLAB Simulink® has been used for this work simulations. Same power system shown in Fig. 29 and same modifications like the ones used for the Type IV WT were used, ratings are shown in Appendix A. Default model of the DFIG in Fig. 39 includes an a) Induction Generator, b)RSC, c) GSC, d) Coupling Inductance and e) Filter.

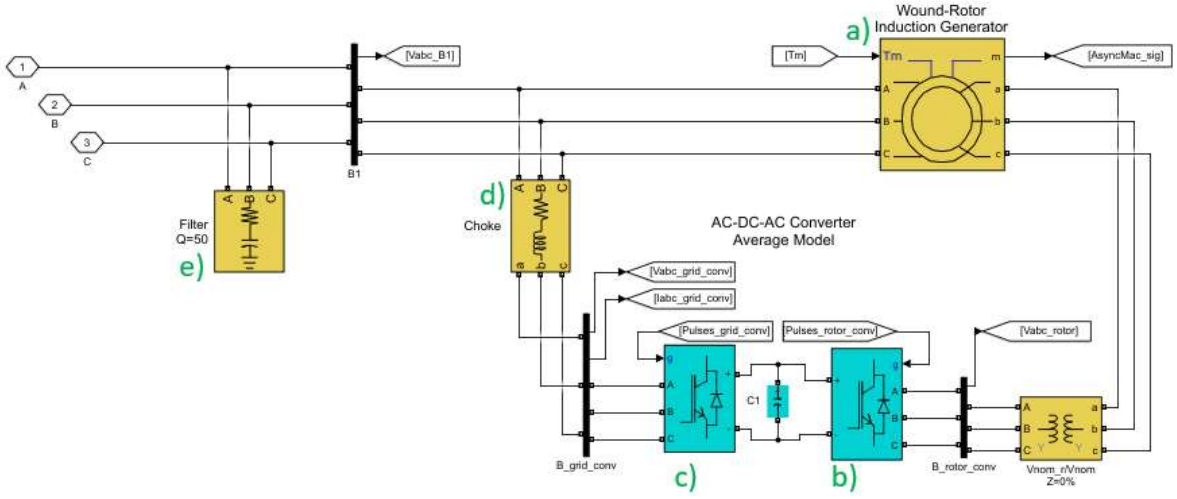

Fig. 39 DFIG MATLAB Simulink Detailed Model

Control System is divided in the following blocks:

- Turbine Speed & Pitch Control. Which due to its slower reaction time is not in the scope of this work due to its limited impact on short circuit response.
- GSC Control. Which includes the Vdc Regulation or Outer Loop and Current Regulator or Inner Loop.
- RSC Control. Which includes the Electromagnetic Torque Controller and Voltage regulator, which, as seen before, constitute the Outer Loop that provides the current reference d and q components respectively and the Current Regulator or Inner Loop.

7.5. Modified Protection Scheme Type III WT Model

As mentioned in Chapter Fault response of IBRs5, on a DFIG Machine, the main impact on fault response is due to the protection method use for the RSC, being it Crowbar or DC Chopper. Modification shown in Fig. 40 were done to the model:

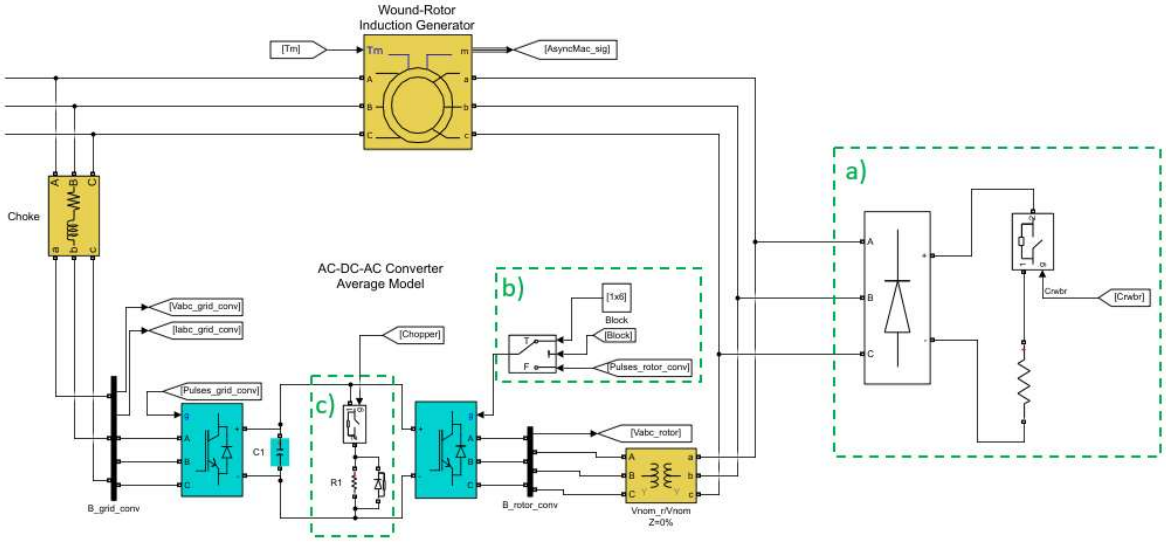

Fig. 40 DFIG Detailed Model with RSC Protection

a) Crowbar system is built by a Diode Bridge an Ideal Switch controlling a resistor. Resistor value has been chosen to 20 times stator resistance as recommended in [51]. Ideal switch receives the command signal from a hysteresis type control which takes in account both rotor phase currents and DC voltage as described in [52], if any of both goes over 1.2 p.u. crowbar is activated and not deactivated until both go under 1.1 p.u. [17], [37].

b) RSC switches are blocked following the same criteria as the crowbar in order to be protected against overcurrent and overvoltage.

c) DC Chopper consists of an ideal switch-controlled resistor in parallel with the DC-link capacitor. DC Chopper resistor was sized according to (29) from [53] taking the power to be dissipated as half of the nominal power of the turbine.

$$P_{break} = \frac{V_{dc}^2}{R_{break}} \tag{30}$$

Different novel control methods have been published aimed to act against the direct flux $\vec{\Psi}_{sf}^{r}$ described on Chapter 5 as the ones listed in [54], including demagnetizing control described in [52] which was implemented but not included on the results of this work since no beneficial results were achieved.

Fig. 41 Impact on DFIG by a ABCG Line Fault without (Left), with protection (Right).Fig. 41 shows the impact on the DFIG by a ABCG Line Fault without any protection technique on the left, and with both Crowbar and DC Chopper protection added. It can be seen how rotor current peak at fault inception are reduced from over 2 p.u. to a lower level under 2 p.u. Vdc is reduced from 1.4 to 1.1 p.u by the draining of the crowbar resistor. Electromagnetic peak is reduced from -2 p.u. to -1.5 p.u. and not allowed to go over cero on the second peak. On the last two graphics, voltage and current along the RSC switches is shown, where it can be seen how voltage is reduced from over 1500V to under 1500V and current peak from 10 kA to 5 kA.

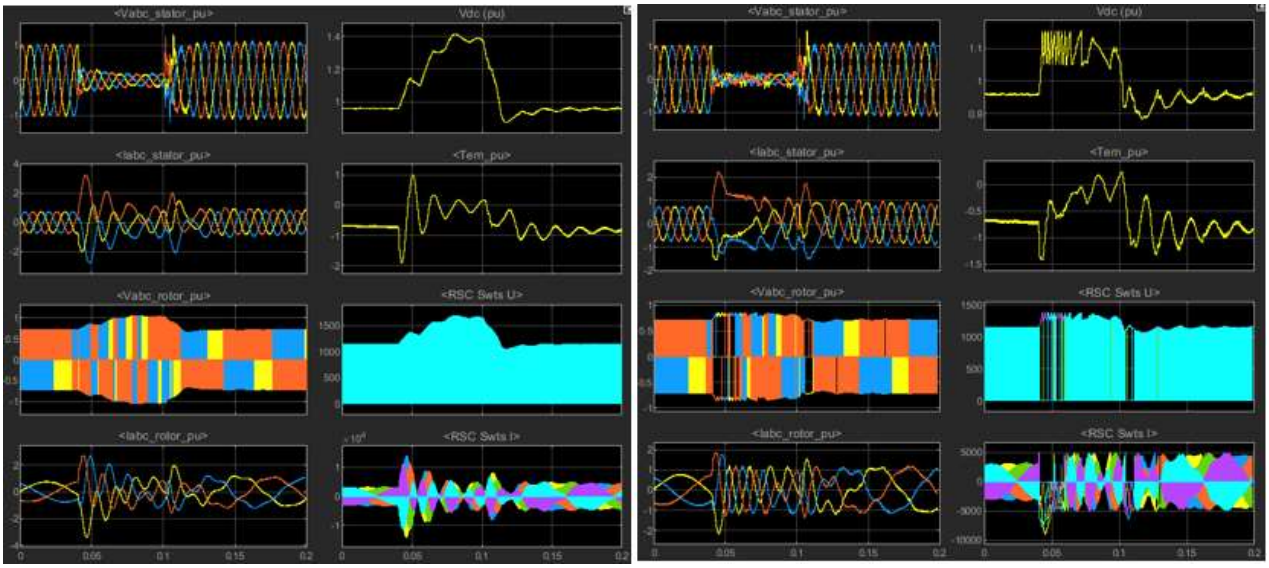

Fig. 41 Impact on DFIG by a ABCG Line Fault without (Left), with protection (Right).

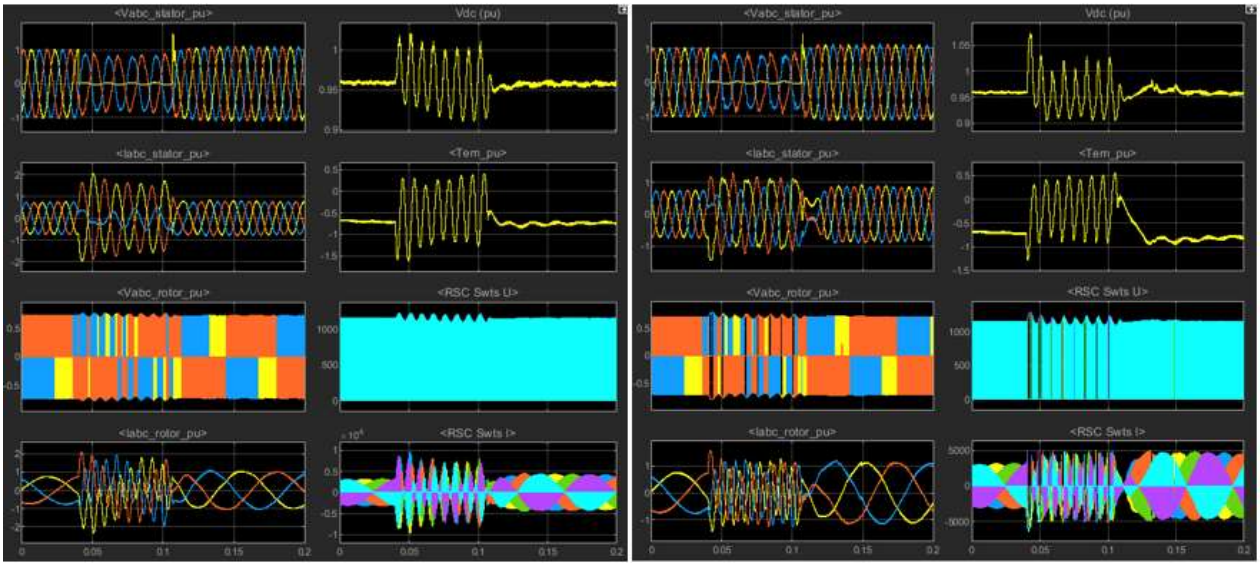

Fig. 42 Impact on DFIG by a AG Fault on Wind Park Terminals without (Left), with protection (Right).

Fig. 42 show impact on the DFIG, but by an asymmetrical AG Fault. In this case the fault had to be simulated right at the Wind Park terminals for the voltage sag to be deep enough for the protections to be activated. The impact of Crowbar and DC Chopper can be seen on the rotor current not reaching the 2 p.u. reaches without protections, which leads to a similar reduction on the RSC switches currents. As mentioned on Chapter 5, the main concern here are the DC Voltage and Torque pulsations. Since both effects are created by the inverse flux and as mentioned in [13], neither crowbar, nor DC Chopper act against this flux, which does not decay with time and remains along the fault. Complex control schemes have been proposed to solve these problems, like tracking inverse flux to inject opposite currents [35] or aiming to either eliminate oscillations of reactive or active power [55].

8. Impact of Wind Turbines on Protection Algorithms

Different faults were simulated at half of the 120 kV line and measurements were done on the end called (WP End), at the Wind Park side of the line.

Results of simulations for different generators and different faults were organized per protection principle for a more understandable presentation. Faults were simulated on a Synchronous Generator for comparison, Type III WT with and without protections (Crowbar and DC Chopper) and Type IV with I2 suppression LVRT mode and I2 injection LVRT mode with different K factors. Results which would hinder protection functions are colored in red, while results that agree with reviewed theory are colored in green.

For the 50Q protection, the magnitude of the negative sequence current is the main parameter to take in account. Results are shown in following table.

Fault	Synchronous Generator	Type III no RSC Protections	Type III with RSC Protections	Type IV (I2 SUPRESSION)	Type IV (I2 INJECTION) K=5	Type IV (I2 INJECTION) K=2
AG	0,8	0,6	0,6	0,3	1,2	1,2
BC	1,6	1,1	1,08	0,5	1,13	1,0
ACG	1,2	0,9	0,8	0,5	1,13	1,13

Table 1 Negative sequence current magnitude (|I2|)

As expected, DFIG shows a similar behavior to synchronous generator since it is directly connected to the stator. For the Type IV WT it is the control systems that dictates I2 behavior, if I2 is suppressed, less than a 0.5 pu of fault current is registered, if I2 injection is taken in account then its level goes over 1 p.u.

Regarding 67Q protection, as previously explained, this function measures impedance on one line end and decides directionality of the current, in the specific case of the 67Q function it takes in account the negative sequence of the current. Following results were obtained for this simulation:

Fault	Grid Side ∠ Z2°	Expected WT Side ∠ Z2°	Synchronous Generator	Type III no RSC Protections	Type III with RSC Protections	Type IV (I2 SUPRESSION)	Type IV (I2 INJECTION) K=5	Type IV (I2 INJECTION) K=2
AG	-90°	90°	78°	80°	85°	10°	-150°	246°
BC	-90	90°	78°	85°	80°	8°	38°	70°
ACG	-90	90°	78°	90°	85°	8°	160°	186°

Table 2 Negative sequence impedance measured at Wind Turbine end of line.

As expected, synchronous generator and Type III WT represents highly inductive impedance near 90°, while Type IV impedance varies among different control methods and K values. This is actually a source of uncertainty for other function calculations as it will be seen forward.

For the Negative and zero sequence current angle comparison FID, the value of **φ** angle as calculated in (25).

Fault	φ Expected	Synch Gen	Type III no RSC Protections	Type III with RSC Protections	Type IV (I2 SUPRESSION)	Type IV (I2 INJECTION) K=5	Type IV (I2 INJECTION) K=2
AG	-30 to +30°	-7°	0°	6°	71°	-125°	-161°
BCG (Rg=10Ohm)	+30° to +90°	41°	50°	36°	33°	0°	-42°
BG	+90 to +150°	109°	115°	122°	-53°	-3°	-70°
ACG	+90 to +150	110°	110°	116°	-43°	-196°	-223°
CG	-90° to -150°	-130°	-125°	-118°	190°	83°	53°

Table 3 Negative and zero sequence current angle φ.

As previously stated, expectation is for the Type III WT to fall under the right angular section for the simulated faults, with similar values to the SG. On the other hand, since current component angular

behavior depends on the impedance represented by the WT to correctly reflect fault voltage behavior, and as previously seen, impedance is variant on the Type IV generator, no reliable results are seen on the Type IV for current FID methods.

For the second current based FID method analyzed, the Negative and positive sequence current angle comparison. The value of calculated Φ angle, per (25) for different fault types is given below:

Fault	Φ Expected	Synch Gen	Type III no RSC Protections	Type III with RSC Protections	Type IV (I2 SUPRESSION)	Type IV (I2 INJECTION) K=5	Type IV (I2 INJECTION) K=2
AG	-30 to +30°	52°	100°	109°	-176°	11°	-45°
CG	-90 to -150°	-60°	-10°	-340°	64°	-37°	-78°
BG	+90 to +150	-190°	-130°	-136°	-40°	0°	-80°
ACG	-90° to -30°	-30°	-310°	60°	160°	22°	-15°
BC	-120° to +120°	-150°	-80°	-67°	26°	37°	-42°

Table 4 Negative and positive sequence current angle Φ

In the case of this specific current based FID method, obtained results did not match the expected values dictated by the reviewed theory. It is interesting to mention that measured values for Synch Generator and Type III WT showed an angular difference of 120° for each variant of fault type. The values did not correspond to the theory and we different for the SG and the DFIG generator but showed the right angular dispersion as shown in Fig. 43. AG, BG and CG Faults are 120° apart, just as ABG, BCG and ACG faults and AB, AC and BC faults for both cases. Further investigation needs to be done on how to match expected values for this FID function like the modified LVRT control for WTs previously mentioned.

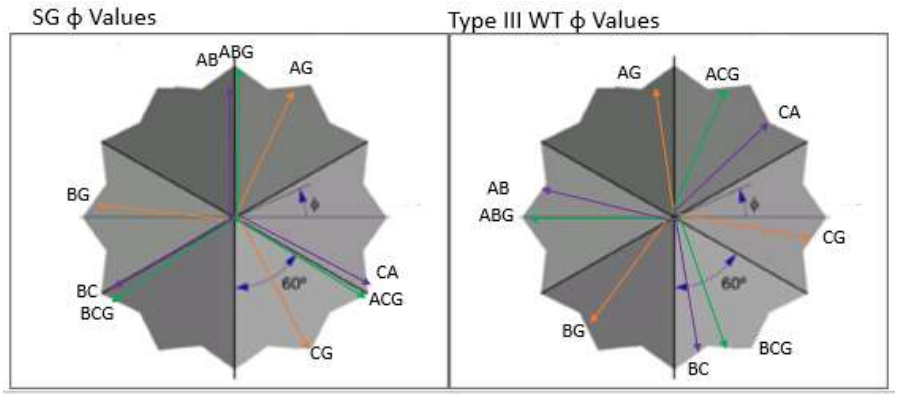

Fig. 43 Angular dispersion for φ values.

As mentioned in [42], due to expected issues with current based FID methods, voltage-based FID functions are of interest. Table 5 Negative and zero sequence voltage method angles Θ and δ Table 5 shows the results obtained for the Negative and zero sequence voltage angle comparison function presented before.

Fault	Expected Θ / δ	Synch Gen	Type III no RSC Protections	Type III with RSC Protections	Type IV (I2 SUPRESSION)	Type IV (I2 INJECTION) K=5	Type IV (I2 INJECTION) K=2
AG	-90° a +30° / |δ | < 90	0°/-180°	0°/180°	356°/173°	-7°/176°	0°/-174°	354°/174°
BG	-90° a -210°/ |δ | < 90	-120°/-60	-120°/61°	-126°/-65°	-125°/-67°	-130/-65°	-130°/-95°
ACG	-90° a -210°/ |δ | > 90	240°/118°	243°/120°	240°/113°	235°/114°	235°/112°	539°/114°
CG	-210 a +30 / |δ | < 90	115°/60°	115°/60°	113°/54°	114°/54°	116°/56°	116°/55°

Table 5 Negative and zero sequence voltage method angles Θ and δ

Results matched previously presented theory, except for the δ angle for AG fault which was consistently showing a value of around 180° when it should have a near 0° value. The most important outcome of this test it that using voltage angle values the measurement is not impacted by the WT type or control characteristics since angular relation between voltage components are dictated by the fault characteristics and not the source.

Finally, Table 6 shows the results for the Negative and Positive Sequence Voltage Angle Comparison method proposed as a way to avoid the effect of the Bauch´s Paradox mentioned in [43]. In this method the angular difference between positive and negative voltage is used to detect fault type and the phase which records an actual low voltage is declared as the faulted one. Simulation showed successful results for the investigated fault types, proving the efficiency of voltage angle-based FIDs.

Fault	Synch Gen		Type III no RSC Protections		Type III with RSC Protections		Type IV (I2 SUPRESSION)		Type IV (I2 INJECTION) K=5		Type IV (I2 INJECTION) K=2	
	°U1-°U2	Ph	°U1-U2	Ph	°U1-U2	Ph	°U1-U2	Ph	°U1-U2	Ph	°U1-U2	Ph
AG	180°	A	180°	A	180°	A	180°	A	-174°	A	180°	A
CG	-60	C	-60°	C	-59°	C	60°	C	-62°	C	-62°	C
BG	60°	B	60°	B	60°	B	60°	B	63°	B	63°	B
ACG	-120°	AC	-120°	AC	-114	AC	-120°	AC	-121°	AC	-121°	AC

Table 6 Negative and positive sequence voltage angle comparison

9. Conclusion

Protection studies have historically been done over the basis that the fault response from the system is known and predictable since it depends on physical characteristics of synchronous generators. As it has been shown in this work, fault response of IBRs is dependent on the type of sources present (Type III Vs Type IV Wind Turbines), the control philosophy (CSC Vs DSC), LVRT protection methods (Crowbar Vs DC Chopper), compliance to the latest grid codes and even PLL technique used. This might bring a higher degree of uncertainty to protection studies.

Regarding the impact of the transformer's connection along the path from fault point to WT, as mentioned in [13], the only effect will be the phase shift for both sequences components, of -30°

and 30° for the positive and negative current sequence for each transformer in the case of our system.

Since, as previously mentioned, the fault response on this new energy sources is heavily determined by their control system, which is usually proprietary and dependent on the inverter manufacturer. Transmission System Operators (TSO) around the globe to stablish a common ground for LVRT requirements on Grid Codes so certainty can be provided to relay manufacturers.

Relay manufacturers also have to adequately invest in understanding IBRs new developments and their impact on protection algorithms used for which stablishing a good communication with inverters and wind turbine manufacturers is highly beneficial.

10. References

[1] ENTSOE, "Short Circuit Contribution of New-Generating Units Connected with Power Electronics and Proteciton Behaviour," April 3rd, 2019.

[2] R. A. Walling *et al*, "Current contributions from Type 3 and Type 4 wind turbine generators during faults," *Proceedings of the IEEE Power Engineering Society Transmission and Distribution Conference,* 2012. Available: https://ehu.on.worldcat.org/oclc/816102796. DOI: 10.1109/TDC.2012.6281623.

[3] Abdul W. Korai *et al*, "Generic DSL-Based Modeling and Control of Wind Turbine Type 4 for EMT Simulations in DIgSILENT PowerFactory," *Advanced Smart Grid Functionalities Based on PowerFactory,* pp. 355-371, 2018. Available: https://link-springer-com.ehu.idm.oclc.org/chapter/10.1007/978-3-319-50532-9_14. DOI: 10.1007/978-3-319-50532-9_14.

[4] V. Akhmatov *et al*, "Siemens Wind Power Variable-Speed Full Scale Frequency Converter Wind Turbine Model for Balanced and Unbalanced Short-Circuit Faults," *Wind Eng,* vol. 34, *(2),* pp. 139-156, 2010. Available: https://doi-org.ehu.idm.oclc.org/10.1260/0309-524X.34.2.139. DOI: 10.1260/0309-524X.34.2.139.

[5] E. Farantatos *et al*, "Short-circuit current contribution of converter interfaced wind turbines and the impact on system protection," *2013 IREP Symposium Bulk Power System Dynamics and Control - IX Optimization, Security and Control of the Emerging Power Grid,* pp. 1-9, 2013.

[6] S. Seman *et al*, "Low voltage ride-through analysis of 2 MW DFIG wind turbine - grid code compliance validations," *2008 IEEE Power and Energy Society General Meeting - Conversion and Delivery of Electrical Energy in the 21st Century,* pp. 1-6, 2008. . DOI: 10.1109/PES.2008.4596687.

[7] T. Y. Zheng *et al*, "Protection algorithm for a wind turbine generator in a large wind farm," *2011 IEEE Trondheim PowerTech,* pp. 1-6, 2011. . DOI: 10.1109/PTC.2011.6019337.

[8] C. CIGRE, "Modelling of inverted-based generation for power system dynamic studies," MAY. 2018.

[9] T. Neumann and I. Erlich, "Modelling and control of photovoltaic inverter systems with respect to German grid code requirements," *2012 IEEE Power and Energy Society General Meeting,* pp. 1-8, 2012. . DOI: 10.1109/PESGM.2012.6345310.

[10] Ö. Göksu *et al*, "Impact of wind power plant reactive current injection during asymmetrical grid faults," *IET Renewable Power Generation,* vol. 7, *(5),* pp. 484-492, 2013. . DOI: 10.1049/iet-rpg.2012.0255.

[11] A. Camacho *et al*, "Positive and Negative Sequence Control Strategies to Maximize the Voltage Support in Resistive-Inductive Grids During Grid Faults," *Ieee Transactions on Power Electronics Pe,* vol. 33, *(6),* pp. 5362-5373, 2018. Available: https://ehu.on.worldcat.org/oclc/7378425267.

[12] S. Alepuz *et al*, "Control Strategies Based on Symmetrical Components for Grid-Connected Converters Under Voltage Dips," *IEEE Trans. Ind. Electron.,* vol. 56, *(6),* pp. 2162-2173, 2009. Available: https://ehu.on.worldcat.org/oclc/423641166.

[13] J. Lopez Taberna, "Comportamiento De Generadores Eólicos Con Máquina Asíncrona Doblemente Alimentada Frente a Huecos De Tensión." , Universidad Pública de Navarra, 2008.

[14] J. González and R. Lacal Arantegui, "Technological evolution of onshore wind turbines—a market-based analysis," *Wind Energy,* 2016. . DOI: 10.1002/we.1974.

[15] R. Teodorescu *et al*, *Grid Converters for Photovoltaic and Wind Power Systems.* John Wiley & Sons, 2011.

[16] Microsemi Corporation, "Park, Inverse Park and Clarke, Inverse Clarke Transformations MSS Software Implementation," 2013.

[17] N. Tleis, "6 - Modelling of voltage-source inverters, wind turbine and solar photovoltaic (PV) generators," *Power Systems Modelling and Fault Analysis (Second Edition),* pp. 469-596, 2019. Available: http://www.sciencedirect.com/science/article/pii/B9780128151174000060. DOI: https://doi.org/10.1016/B978-0-12-815117-4.00006-0.

[18] R. Teodorescu *et al*, "Proportional-resonant controllers and filters for grid-connected voltage-source converters," *IEE Proceedings - Electric Power Applications,* vol. 153, *(5),* pp. 750-762, 2006. . DOI: 10.1049/ip-epa:20060008.

[19] Hemami and Ahmad, *Electricity and Electronics for Renewable Energy Technology.* (1st ed.) 2017Available: https://www.taylorfrancis.com/books/9781315275062. DOI: 10.4324/9781315275062.

[20] Yongheng Yang, Wenjie Chen and Frede Blaabjerg, "Advanced control of photovoltaic and wind turbines power systems," in *Advanced and Intelligent Control in Power Electronics and Drives, Studies in Computational Intelligence*Anonymous Springer International Publishing Switzerland, 2014, .

[21] R. Kabiri, D. G. Holmes and B. P. McGrath, "Double synchronous frame current regulation of distributed generation systems under unbalanced voltage conditions without sequence current separation," in *2015 IEEE Applied Power Electronics Conference and Exposition (APEC),* 2015, . DOI: 10.1109/APEC.2015.7104594.

[22] T. Kauffmann *et al*, "Short-Circuit Model for Type-IV Wind Turbine Generators With Decoupled Sequence Control," *IEEE Transactions on Power Delivery,* vol. 34, *(5),* pp. 1998-2007, 2019. . DOI: 10.1109/TPWRD.2019.2908686.

[23] J. Zhou *et al*, "Active power decoupling methods for three-phase grid-connected converters under unbalanced grid conditions," *2017 IEEE 18th Workshop on Control and Modeling for Power Electronics (COMPEL),* pp. 1-7, 2017. . DOI: 10.1109/COMPEL.2017.8013303.

[24] T. Neumann *et al*, "Enhanced Dynamic Voltage Control of Type 4 Wind Turbines During Unbalanced Grid Faults," *IEEE Transactions on Energy Conversion,* vol. 30, *(4),* pp. 1650-1659, 2015. . DOI: 10.1109/TEC.2015.2470126.

[25] E. G. Shehata, "Direct power control of wind-turbine-driven DFIG during transient grid voltage unbalance," *Wind Energy,* vol. 17, *(7),* pp. 1077-1091, 2014. Available: https://onlinelibrary-wiley-com.ehu.idm.oclc.org/doi/abs/10.1002/we.1619. DOI: 10.1002/we.1619.

[26] A. HADDADI *et al*, "Field validation of generic wind park models using fault records," *J. Mod. Power Syst. Clean Energy,* vol. 7, *(4),* pp. 826-836, 2019. Available: https://search.proquest.com/docview/2205098199. DOI: 10.1007/s40565-019-0521-x.

[27] I. Erlich *et al*, *Wind Turbine Negative Sequence Current Control and its Effect on Power System Protection.* 2013. DOI: 10.1109/PESMG.2013.6672880.

[28] Xiaoqiang Guo *et al*, "Flexible Control Strategy for Grid-Connected Inverter Under Unbalanced Grid Faults Without PLL," *IEEE Transactions on Power Electronics,* vol. 30, *(4),* 2015. Available: https://ehu.on.worldcat.org/oclc/5872832981. DOI: 10.1109/TPEL.2014.2344098.

[29] P. Rodríguez *et al*, "New positive-sequence voltage detector for grid synchronization of power converters under faulty grid conditions," in *2006 37th IEEE Power Electronics Specialists Conference,* 2006, . DOI: 10.1109/pesc.2006.1712059.

[30] V. Vittal and R. Ayyanar, *Grid Integration and Dynamic Impact of Wind Energy.* 2013Available: https://ehu.on.worldcat.org/oclc/802279676. DOI: 10.1007/978-1-4419-9323-6.

[31] J. Machowski *et al*, *Power System Dynamics : Stability and Control.* (2nd ed. ed.) 2008Available: https://ehu.on.worldcat.org/oclc/916030057.

[32] T. Kauffmann *et al*, "An accurate type III wind turbine generator short circuit model for protection applications," in *2017 IEEE Power & Energy Society General Meeting,* 2017, . DOI: 10.1109/PESGM.2017.8274588.

[33] A. D. Hansen *et al*. Dynamic wind turbine models in power system simulation tool DIgSILENT. Danmarks Tekniske Universitet, Risø Nationallaboratoriet for Bæredygtig Energi. 2007Available: https://orbit.dtu.dk/en/publications/dynamic-wind-turbine-models-in-power-system-simulation-tool-digsi-2.

[34] F. K. A. Lima *et al*, "Rotor Voltage Dynamics in the Doubly Fed Induction Generator During Grid Faults," *IEEE Transactions on Power Electronics,* vol. 25, *(1),* pp. 118-130, 2010. . DOI: 10.1109/TPEL.2009.2025651.

[35] J. Rodríguez Arribas *et al*, "Low Voltage Ride-through in DFIG Wind Generators by Controlling the Rotor Current without Crowbars," *Energies,* vol. 7, *(2),* pp. 498-519, 2014. Available: http://www.mdpi.com/1996-1073/7/2/498.

[36] Y. Zhou *et al*, "Operation of Grid-Connected DFIG Under Unbalanced Grid Voltage Condition," *IEEE Transactions on Energy Conversion,* vol. 24, *(1),* pp. 240-246, 2009. . DOI: 10.1109/TEC.2008.2011833.

[37] Maoze Wang *et al*, "A new control system to strengthen the LVRT capacity of DFIG based on both crowbar and DC chopper circuits," in *IEEE PES Innovative Smart Grid Technologies,* 2012, . DOI: 10.1109/ISGT-Asia.2012.6303234.

[38] J. Hossain and A. Mahmud, *Large Scale Renewable Power Generation : Advances in Technologies for Generation, Transmission and Storage.* 2014Available: https://ehu.on.worldcat.org/oclc/870308720. DOI: 10.1007/978-981-4585-30-9.

[39] ZIV APLICACIONES Y TECNOLOGÍA, "Manual de Instrucciones para Modelos ZLF," 2019.

[40] Z. Y. Xu *et al*, "Fault phase selection scheme of EHV/UHV transmission line protection for high-resistance faults," *IET Generation, Transmission & Distribution,* vol. 6, *(11),* pp. 1180-1187, 2013. Available: https://ehu.on.worldcat.org/oclc/8540471197.

[41] J. D. Glover, M. S. Sarma and T. J. Overbye, *Power System Analysis & Design.* (5th ed.) Stamford, CT, USA: Cengage Learning, 2011.

[42] Shaofeng Huang, Lan Luo and Kai Cao, "A Novel Method of Ground Fault Phase Selection in Weak-Infeed Side," *IEEE Trans. Power Del.,* vol. 29, *(5),* 2014. Available: https://ehu.on.worldcat.org/oclc/5872829835. DOI: 10.1109/TPWRD.2014.2322073.

[43] C. Dzienis *et al*, "A method for the correct protection response during power system faults subjected to the bauch's paradox phenomenon," in *23rd International Conference on Electricity Distribution,* 2015, .

[44] P. Horton and S. Swain, "Using Superimposed Principles (Delta) in Protection Techniques in an Increasingly Challenging Power Network," .

[45] G. Benmouya and J. Roberts, "Superimposed quantities: Their true nature and application in relays," in *26th Annual Western Protective Relay Conference,* pp. 1-19.

[46] M. M. Shabestary and Y. A. I. Mohamed, "Asymmetrical Ride-Through and Grid Support in Converter-Interfaced DG Units Under Unbalanced Conditions," *IEEE Transactions on Industrial Electronics,* vol. 66, *(2),* pp. 1130-1141, 2019. . DOI: 10.1109/TIE.2018.2835371.

[47] T. Wijnhoven *et al*, "Control aspects of the dynamic negative sequence current injection of type 4 wind turbines," in *2014 IEEE PES General Meeting | Conference & Exposition,* 2014, . DOI: 10.1109/PESGM.2014.6938931.

[48] Industry, Tourism and Commerce Spanish Ministry, ""“Operation Procedure O.P. 12.2: Response requirements in front of voltage dip at wind farms utilities." May, 17, 2018.

[49] A. Haddadi *et al*, "Negative sequence quantities-based protection under inverter-based resources Challenges and impact of the German grid code," *Electr. Power Syst. Res.,* vol. 188, pp. 106573, 2020. Available: http://www.sciencedirect.com.ehu.idm.oclc.org/science/article/pii/S0378779620303771. DOI: https://doi-org.ehu.idm.oclc.org/10.1016/j.epsr.2020.106573.

[50] M. A. Azzouz and A. Hooshyar, "Dual Current Control of Inverter-Interfaced Renewable Energy Sources for Precise Phase Selection," *IEEE Transactions on Smart Grid,* vol. 10, *(5),* pp. 5092-5102, 2019. . DOI: 10.1109/TSG.2018.2875422.

[51] G. N. Sava *et al*, "Comparison of active crowbar protection schemes for DFIGs wind turbines," in *2014 16th International Conference on Harmonics and Quality of Power (ICHQP),* 2014, . DOI: 10.1109/ICHQP.2014.6842860.

[52] L. Peng, B. Francois and Y. Li, "Improved crowbar control strategy of DFIG based wind turbines for grid fault ride-through," in *2009 Twenty-Fourth Annual IEEE Applied Power Electronics Conference and Exposition,* 2009, . DOI: 10.1109/APEC.2009.4802937.

[53] G. Pannell *et al*, "Evaluation of the Performance of a DC-Link Brake Chopper as a DFIG Low-Voltage Fault-Ride-Through Device," *IEEE Transactions on Energy Conversion,* vol. 28, *(3),* pp. 535-542, 2013. . DOI: 10.1109/TEC.2013.2261301.

[54] O. P. Mahela *et al*, "Comprehensive Overview of Low Voltage Ride Through Methods of Grid Integrated Wind Generator," *IEEE Access,* vol. 7, pp. 99299-99326, 2019. . DOI: 10.1109/ACCESS.2019.2930413.

[55] R. Kabiri, D. G. Holmes and B. P. McGrath, "Control of distributed generation systems under unbalanced voltage conditions," in *2014 International Power Electronics Conference (IPEC-Hiroshima 2014 - ECCE ASIA),* 2014, . DOI: 10.1109/IPEC.2014.6870161.

Annex A

Grid			MV Cable			Type IV WT		
Frequency	60	Hz	R1	0,1153	Ω/km	Wind Turbines	5	

Low Voltage	0,575	kV
Medium Voltage	25	kV
High Voltage	120	kV

MV/LV Transformer		
Connection	D11/Yg	
Nominal Power	1,75*6	MVA
R	0,00083	pu
L	0,025	pu
Rm	500	pu

HV/MV Transformer		
Connection	Yg/D1	
Nominal Power	4,70E+01	MVA
R	0,0027	pu
L	0,08	pu
Rm	500	pu

Grounding Transformer		
Nominal Power	100	MW
R0	0,0265	pu
X0	0,75	pu
Rm	500	pu
Xm	500	pu

R0	0,413	Ω/km
L1	1,05E-03	H/Km
L0	3,32E-03	H/Km
C1	1,13E-08	F/Km
C0	5,01E-09	F/Km
Length	5	km

HV Line		
R1	0,176	Ω/km
R0	0,42	Ω/km
L1	1,57E-03	H/Km
L0	3,82E-03	H/Km
C1	1,13E-08	F/Km
C0	5,01E-09	F/Km
Lenght	30	km

Type III WT		
Wind Turbines	6	
Nominal Power	1,5	MW
Frequency	60	Hz
Vstator	575	V
Vrotor	1975	V
R stator	0,023	pu
L stator	0,18	pu
R rotor	0,016	pu
L rotor	0,16	pu
L magnetizing	2,9	pu
Inertia constant (H)	0,685	s
Friction Factor (F)	0,01	pu
Pole pair (p)	3	

Nominal Power	2	MW
Frequency	60	Hz
Vstator	730	V
Xd	1,305	pu
Xd´	0,296	pu
Xd´´	0,252	pu
Xq	0,474	pu
Xq´´	0,243	pu
Xl	0,18	pu
Tdo´	4,49	pu
Tdo´´	0,0618	pu
Tq´´	0,0513	pu
R stator	0,006	pu
Inertia constant (H)	0,62	s
Friction Factor (F)	0,01	pu
Pole pair (p)	1	